SIMULTANEOUS STM / nc-AFM INVESTIGATION OF CLEAN Si(001)-(2×1) SURFACE AND Ge EPITAXIAL GROWTH ON Si(001)-(2×1)

A THESIS

SUBMITTED TO THE DEPARTMENT OF PHYSICS

AND THE INSTITUTE OF ENGINEERING AND SCIENCE

OF BILKENT UNIVERSITY

IN PARTIAL FULFILLMENT OF THE REQUIREMENTS

FOR THE DEGREE OF

MASTER OF SCIENCE

By

Mehrdad Atabak

September 2001

I certify that I have read this thesis and that in my opinion it is fully adequate, in scope and in quality, as a dissertation for the degree of Master of Science.

Asst. Prof. Ahmet Oral (Supervisor)

I certify that I have read this thesis and that in my opinion it is fully adequate, in scope and in quality, as a dissertation for the degree of Master of Science.

Assoc. Prof. Recai M. Ellialtıoğlu

I certify that I have read this thesis and that in my opinion it is fully adequate, in scope and in quality, as a dissertation for the degree of Master of Science.

Asst. Prof. Serdar Özçelik

Approved for the Institute of Engineering and Science:

Prof. Mehmet Baray,
Director of Institute of Engineering and Science

Abstract

SIMULTANEOUS STM/NC-AFM INVESTIGATION OF CLEAN SI(001)-(2 × 1) SURFACE AND GE EPITAXIAL GROWTH ON SI(001)-(2 × 1)

Mehrdad Atabak
M. S. in Physics
Supervisor: Asst. Prof. Ahmet Oral
September 2001

In this thesis work, a combined Scanning Tunnelling Microscope and non-contact Atomic Force Microscope -STM/ncAFM- is used to investigate clean Si(001)-(2 × 1) and Ge epitaxial growth on Si(001)-(2 × 1) surfaces.
The STM/nc-AFM and Ultra High Vacuum system (UHV) in which the microscope is installed, are also described.
The capability of our new microscope to image the clean Si(001) and Ge epitaxial growth on Si(001) and force-distance spectroscopy on Si(001) is demonstrated.

Keywords: Ultra High Vacuum, Scanning Tunnelling Microscopy, Atomic Force Microscopy, Force-Distance Spectroscopy, Epitaxial growth.

Özet

TEMİZ Si(001)-(2×1) YÜZEYİ VE ÜZERİNE EŞÖRGÜSEL GE TABAKASI BÜYÜTÜLMÜŞ Si(001)-(2×1) YÜZEYLERİNİN TARAMALI TÜNELLEME MİKROSKOBU VE TEMASSIZ ATOMİK KUVVET MİKROSKOBUNUN EŞZAMANLI KULLANILARAK İNCELENMESİ

Mehrdad Atabak
Fizik Yüksek Lisans
Tez Yöneticisi: Asst. Prof. Ahmet Oral
Eylül 2001

Bu tez çalışmasında, taramalı tünelleme mikroskobu (TTM) ve temassız atomik kuvvet mikroskobu (temassız-AKM) , temiz Si(001)-(2×1) yüzeylerinin ve üzerinde eşörgüsel büyütülmüş germanyum olan Si(001)-(2×1) yüzeylerinin incelenmesinde birlikte kullanılmıştır. TTM/temassız-AKM ve mikroskobun içine kurulduğu ultra yüksek vakum sistemi tanıtıldı. Bu mikroskobun temiz Si(001) yüzeyini ve üzerinde eşörgüsel germanyum büyütülmüş Si(001) yüzeyini ve Si(001)'in kuvvet-uzaklık tayfını görüntülemekteki kapasitesi gösterildi.

Anahtar sözcükler: Ultra Yüksek Vakum Sistemi, Taramalı Tünelleme Mikroskobu, Atomik Kuvvet Mikroskobu, Kuvvet-Uzaklık Tayfı, Eşörgüsel Büyüme.

Acknowledgement

I would like to express my sincere gratitude to my supervisor Asst. Prof. Dr. Ahmet Oral. This work would not have been possible without his expertise and support. Beyond that, with his motivating and friendly attitude, I feel myself lucky to be his graduate student.

I also owe special thanks to Dr. H. Özgür Özer for his helps, supplying me the experimental tools and his valuable remarks on the problems during experiment.

I would like to thank Assoc. Prof. Recai M. Ellialtıoğlu and Asst. Prof. Serdar Özçelik for reading the manuscript and offering fine suggestions.

I would also like to thank to my great friend, Mohammad Reza dodge. Although he is far away, but I always feel his existence is my life source.

I greatfully acknowledge to Münir Dede and Sinan Selçuk, who patiently helped me during this thesis. I would also like to thank my friends, Önur, Engin, Ayhan, Murat, Mehmet , Ertuğrul, Irfan and my other friends.

I am also indebted to my mom, my dad and my brothers for their encouragement and love.

And especially, my love and thanks go to *Mehrnaz* for her love and patience.

Contents

List of Figures

Chapter 1

Introduction

The physical, chemical and technical tasks on the nanometer scale, addressed with the help of Scanning Tunnelling Microscopy(STM)[1,2] and AFM,[3] constitute a very broad and dynamic field. The Atomic Force Microscope (AFM) was developed In 1986, a few years after the invention of the Scanning Tunnelling Microscope by Binnig and Rohrer. In the AFM, tip-sample forces are used to obtain surface topography of the sample. In contrast to STM, sample conductivity was no longer a requirement, and therefore insulators and large band-gap semiconductors, were brought into the realm of atomic-scale Scanning Probe measurements.

The Atomic Force Microscope[3] not only opened up a new possibility of imaging surfaces using forces, but also determine the basic physical properties of materials such as adhesion, friction and lubrication,[4] as well as the interactions between biological entities such as proteins, DNA and cells.
This chapter is intended to give an introduction to Scanning Tunnelling Microscope and Atomic Force Microscope as surface imaging techniques that can give atomic resolution images.

1.1 The Scanning Tunnelling Microscope(STM)

In 1980 Binnig and Rohrer designed a fascinating new microscope, which is based on a quantum mechanical phenomenon, *electron tunnelling*. Electron

tunnelling represents the transition of an electron from one classically allowed region into another one, when they are separated by a potential barrier to the classical movement, where the energy of the electron is lower than the barrier potential as shown in Figure 1.1. In the STM, electrons tunnel through a vacuum gap which separates the sharp metal tip from the sample surface. The wave nature of electrons is invoked in the theoretical description of tunnelling and the transmission probability for a wave incident on a one- dimensional barrier can be calculated.

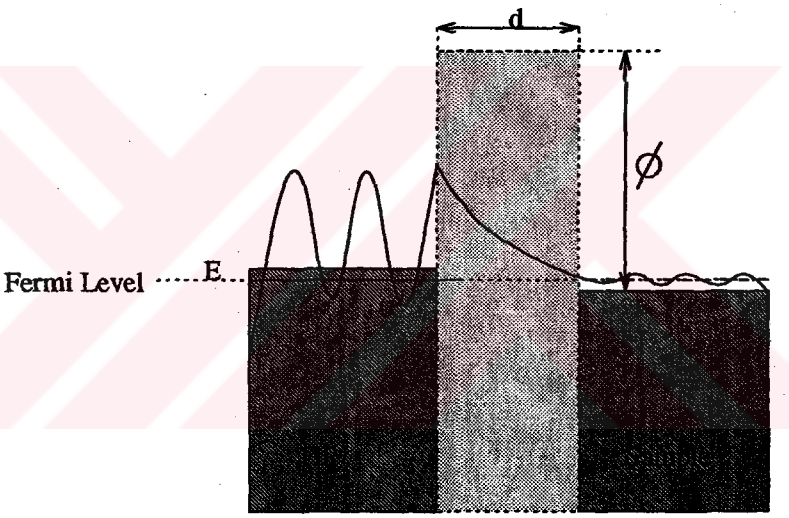

Figure 1.1: Schematic view of a one dimensional tunnelling barrier

The solutions of Schrödinger's equation inside a rectangular barrier in one dimension[6] have the form

$$\psi = \exp(-kz) \tag{1.1}$$

Where the decay length,k , is:

$$k = \sqrt{2m(\phi - E)}/\hbar \tag{1.2}$$

Where E is the energy of incident particle, and ϕ is the barrier hight. The tunnelling current which is proportional to the transmission probability through

the potential barrier width d can be calculated as:

$$I \propto \exp(-2kd) \tag{1.3}$$

In the STM, electrons tunnel through a vacuum gap which separates the sharp metal tip from the sample surface. If a bias voltage is applied, the Fermi level of one of them is shifted relative to the other one, therefore the electrons can tunnel from filled tip states into the empty sample state into the empty states.

1.1.1 Topographic Imaging by STM

STM can be operated on two modes. Constant current mode and constant hight mode.

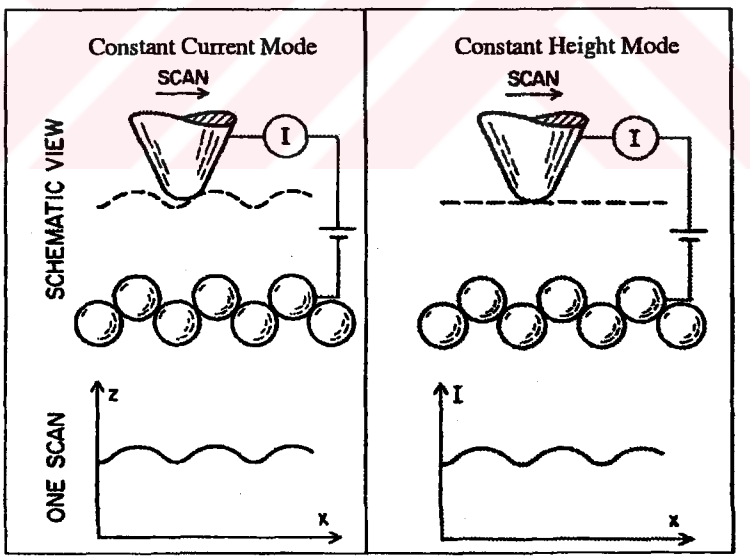

Figure 1.2: Schematic view of constant current mode and constant height mode STM.

In the constant current mode, as shown in Figure 1.2, the tip scans over surface, while the tunnelling current is kept constant, using a feedback circuit

while scanning the surface.

The feedback circuit generates appropriate voltages (V_z) to the z piezo in order to keep the tunnel current constant, while the lateral tip scanned by applying appropriate voltages, V_x and V_y to the x and y piezoelectric scanner. Therefore, one can obtain the topography $z(x, y)$ of the sample by recording $V_z(x, z)$.

In the constant height mode, the tip is kept at constant hight during the scan and the current is recorded, the feedback only maintains an average tunnelling current. The current variations are recorded to obtain surface structure. The constant hight mode which can be run quite fast, offers the opportunity to observe dynamic atomic- scale processes at surfaces, such as surface diffusion, etc. On the other hand, the constant current mode is more reliable to scan surfaces which contains steps and ad-atoms.

1.1.2 Theory of STM

STM is based on electron tunnelling, the images correspond to changes in local density of states at the Fermi level. Tersoff and Hamann developed[7] a simple theory of STM. They used Bardeen's transfer Hamiltonian formalism[8,9] to derive an expression for the current.

$$I = \frac{2\pi e}{h} \sum_{\mu,\nu} f(E_\mu)[1 - f(E_\nu + eV)]|M_{\mu\nu}|^2 \delta(E\mu - E\nu) \tag{1.4}$$

Where the *f(E)* is the Fermi-Dirac distribution function, $M_{\mu\nu}$ is the tunnelling matrix element between the states of the metal tip, ψ_μ , and of the sample surface, ψ_ν:

$$M_{\mu\nu} = -\frac{\hbar^2}{2m} \int d\vec{s} (\psi_\mu^* \nabla \psi_\nu - \psi_\nu^* \nabla \psi_\mu) \tag{1.5}$$

E_μ and E_ν are the energies of the states in the absence of the tunnelling and V is the sample bias voltage. This expression can be simplified into the following form:

$$I \propto \sum_\nu |\psi_\nu(\vec{r_\circ})|^2 \delta(E_\nu - E_f) \tag{1.6}$$

The right hand side is the surface local density of states (LDOS) at the Fermi level E_f at the position $\vec{r_o}$ of the tip $\rho(E_f, \vec{r_o})$. The tunnelling current is not directly related to the position of atomic nuclei but related to the local density of states at the Fermi level. Tersoff-Hamann theory is valid for the tunnelling between s-type states in the absence of significant tip- sample interaction effects.

1.2 Atomic Force Microscopy(AFM)

Atomic Force Microscopy[3] invented by Binnig, Quate and Gerber in 1986 as a tool for studying insulating and conducting surfaces. Basic ingredients of an Atomic Force Microscope is shown in Fig. 1.3.

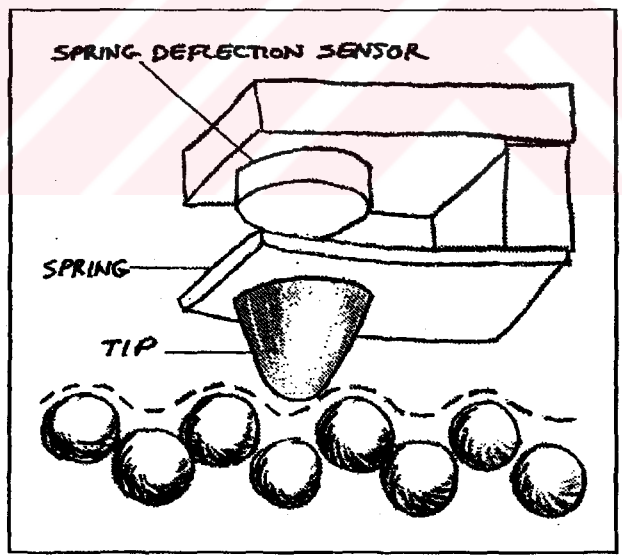

Figure 1.3: Scheme for an Atomic Force Microscope

In fact, the concept of using a force to image a surface is a general one, and can be applied to magnetic and electrostatic forces as well as the interatomic interaction between the tip and the sample. Whatever the origin of the force, all

force microscopes have five essential components:

- A sharp tip integrated to a cantilever spring
- A way of sensing the cantilever deflection
- A feedback system to monitor an the deflection (and, hence, the interaction force)
- A mechanical scanning system (usually piezoelectric crystal based system)
- A control and image system that converts the measured data into an image.

The scanning, feedback and display systems are very similar to those used for STM.

An AFM can be operated in three modes: contact mode, non-contact mode and intermittent-contact mode. Fig. 1.4 shows the operative region of each mode, on a typical interatomic force-distance curve.

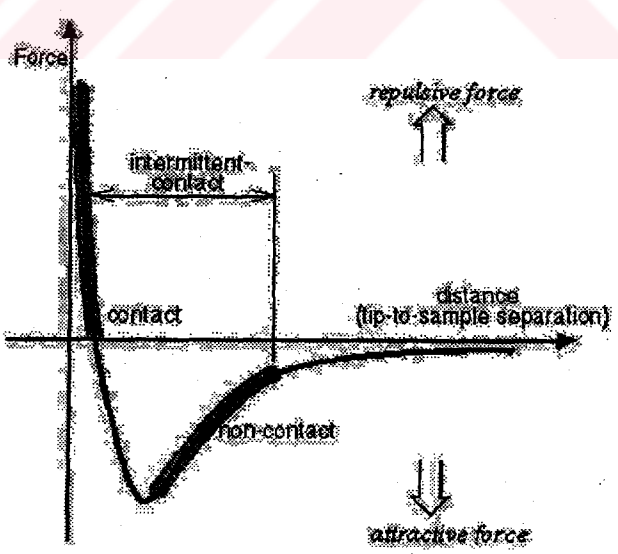

Figure 1.4: Interatomic force vs. distance curve.

In contact mode the tip is in contact with the sample, and repulsive forces between the tip and sample are measured. The total tip-surface force is the sum of both large range van der Waals (vdW) and short range chemical interactions. For distances below 2 Å, the chemical interaction is dominated by the Pauli repulsion and starts to balance the attractive vdW force. AFM images taken at small tip-surface distances, where the total tip-surface force is repulsive(the vdW interaction is smaller than the short range atomic repulsion), are said to be formed during contact mode. Atomic resolution images of layered material such as graphite and boron nitride have been reported[19] but the images rarely show individual surface defects, which are routinely observed with the STM. Furthermore, these images persist at large forces (100 nN) where the contact area is predicted to be of the order of 100 Å^2. These results suggest that both tip and sample are deformed by the repulsive interaction and that the tip is far from being single atom tip which needed for real atomic resolution.

In non-contact AFM mode, the tip is not in contact with the sample, and long-range interaction forces, e.g. vdW, electrostatic, and magnetic force can also be probed. Unlike contact mode, this method is sensitive to force gradient, rather than the interaction forces between tip and sample. The cantilever is driven to vibrate at its resonance frequency by means of a piezoelectric element, and changes in the resonant frequency as a result of tip-sample interaction are measured. The force gradient $F' = -\partial F_z/\partial z$ results in a modification of the effective spring constant of the cantilever

$$k_{eff} = k - F' \tag{1.7}$$

Where k is the spring constant of cantilever in the absence of tip-surface force interaction. An attractive tip-surface interaction with ($F' > 0$) will therefore soften the effective spring constant ($k_{eff} < k$), whereas a repulsive tip-surface force interaction ($F' < 0$) will strengthen the effective spring constant ($k_{eff} > k$). The change of the effective spring constant, in turn, a shift in the resonant

frequency ω of the cantilever according to

$$\omega = (\frac{k_{eff}}{m})^{1/2} = [\frac{(k - F')}{m}]^{1/2} = (\frac{k}{m})^{1/2}(1 - \frac{F'}{k})^{1/2} = \omega_o(1 - \frac{F'}{k})^{1/2} \quad (1.8)$$

where m is an effective mass and ω_o is the resonance frequency of the cantilever in the absence of force gradient. If F' is small relative to k then the Eq.(1.4) can be approximated by

$$\omega \approx \omega_o(1 - \frac{F'}{2k}) \quad (1.9)$$

and therefore

$$\frac{\Delta\omega}{\omega_o} \approx -\frac{F'}{2k} \quad (1.10)$$

and attractive force with ($F' > 0$) will therefore lead to a decrease of the resonant frequency ($\omega < \omega_o$), whereas a repulsive force ($F' < 0$) will lead to an increase ($\omega > \omega_o$).

The above approximation can be to applied to small cantilever oscillation amplitude A, compared to the length scale of the tip-surface interaction force. However most non-contact AFMs operate at very large oscillation amplitudes, 1-60 nm! if the maximum restoring force is greater than the maximum attractive force, $kA \gg F_{max}$, and the cantilever is driven at its resonance frequency, the shift of resonance frequency $\Delta\omega$ can be described by the following perturbation equation:

$$\frac{\Delta\omega}{\omega_o} kA = \int_0^{2\pi} \frac{d\varphi}{2\pi} F(\overline{z} + A\cos\varphi)\cos\varphi \quad (1.11)$$

where the force F is integrated over one oscillation cycle and $\overline{z}$ is the time averaged position of the tip.

Different methods are used for measurement of the resonance frequency shift, Δf. A method which is called slope detection method, the cantilever is driven by means of a piezoelectric element with a typical amplitude at the tip on the order of 1-10 nm at a determined frequency ω_d, the amplitude change or phase shift of the vibration as a result of the tip-surface force interaction is measured with the deflection sensor and a lock-in amplifier. A feedback loop adjusts the tip-surface separation by maintaining a constant force gradient. Another method which is proposed by Albrecht *et al.*[10] in 1991 is called frequency modulation

(FM) technique, oscillation of the cantilever is maintained by a feedback loop using the signal from deflection sensor. Change in the oscillation frequency, caused by variations of the force gradient of the tip sample interaction, are directly measured by a frequency counter or FM discriminator. To achieve the highest possible detection sensitivity for a given free oscillation amplitude A_o, the cantilever should have a small spring constant k and a high resonance frequency f_o, in addition, a high Q-factor for the cantilever is desirable, which only can be achieved in the vacuum condition.

Oral *et al.*[20–24] proposed a new non-contact measurement that directly measure the force gradient of the tip- surface interaction using very small oscillation amplitude of less than 0.25 Å. In this limit the measurement is linear and quasi-static. This enables the researchers to directly measure the force gradient curves up to the contact regime. This technique overcomes some of the limitations of the nc-AFMs, which use large amplitude frequency modulation techniques. While providing high resolution images these techniques have limitation to give quantitative spectroscopic data in atomic manipulation experiments and in measuring the nature of dissipative processes which lie at the heart of nanotechnology. This is because the measured parameter(frequency shift Δf) is not related to the interaction energy or force in a simple manner . Mathematical deconvolution is needed in order to extract the force,[12–16] which relies on a number of assumptions such as the harmonic motion of the lever, a conservation interaction potential and general reversibility of the interaction. In low amplitude nc-AFM technique, the maximum possible energy input into the tip-sample interaction region is of the order of only 10^{-3} eV per cycle as opposed to several eV in the case of large amplitude, resonance enhancement technique. In addition, a high Q-factor cantilever and vacuum condition is no longer a requirement, therefore this technique promises to explore and map the mechanics of matter at the nano-and atomic scale even in ambient condition and under liquids.[25,26]

In intermittent-contact atomic force microscopy which is similar to nc-AFM, the cantilever tip is brought closer to the sample so that the bottom of its travel

it just barely hits, or "taps", the sample. As for nc-AFM, for intermittent-contact atomic force microscopy the cantilever's oscillation amplitude changes in response to tip-to-sample spacing. An image representing surface topography is obtained by monitoring these changes. Some samples are best handled using IC-AFM instead of contact or non-contact AFM. IC-AFM is less likely to damage the sample than contact AFM because it eliminates lateral forces (e.g. friction) between the tip and the sample. In general, it has been found that IC-AFM is more effective than nc-AFM for imaging larger scan sizes that may include greater variation in sample topography.

1.2.1 Measuring the Cantilever Deflection

Different techniques have been employed for measurement the deflection of the cantilever and each technique has advantages and disadvantages. The following sections give brief introduction on different methods.

Tunnelling Detection

The first AFM used an STM tip to measure the cantilever detection by Binnig. The STM tip is positioned behind the AFM lever, and used to measure the cantilever displacement. This method is very sensitive to contamination, roughness of the cantilever and to thermal drift, which make it rather unreliable.

Capacitance Detection

This method was first used by Neubauer *et al.*,[37] The back of cantilever is used as one plate in a capacitor. As the lever bends the change in its position results in a change in the capacitance. The variation of the capacitance is measured and used to calculate the deflection of the lever. The sensitivity is dependent on the smoothness and distance between the plates. The sensitivity of this technique to uniform smoothness of surfaces and distance between the plates. The sensitivity of this technique is of the order of 1×10^{-2} Å$/\sqrt{Hz}$

Optical Beam Deflection

This technique is first employed by Meyer and Amer.[38] A laser beam is reflected from the back of the cantilever onto a two-cell photodiode. Force on the tip cause the cantilever to bend, and the position of the reflected laser spot moves, causing a change in the relative intensity of the photodiode signals, this technique was later extended, using a four-cell photodiode to measure the twisting of the cantilever and hence the lateral force on the tip. This technique has a sensitivity of $\sim 5 \times 10^{-3}$Å$/\sqrt{Hz}$

Optical Fiber Based Interferometry

Deflection measurement with optical interferometry[5,43] is the most sensitive and appropriate method for UHV condition, this technique will be described in detail in the next chapter.

Chapter 2

UHV STM/nc-AFM System

2.1 The Ultra High Vacuum System

In order to keep the Si surface clean, all the experiments were carried out under *Ultra High Vacuum* condition- since the semiconductors and metal surfaces oxidize easily in air. The base pressure of the chamber is better than 1×10^{-10} mbar, after bake out at 160 °C for more than 48 hours.

The UHV system is composed of two main parts, preparation/analysis chamber and fast entry lock. The size of the system is kept as small as possible in order to reach better Ultra High Vacuum condition. Schematic view of UHV system is shown in Figure 2.1. The Fast Entry Lock (FEL) allows samples and cantilevers to be transferred in to, or out of, the chamber without breaking the vacuum, the gate valve (GV) isolates the UHV chamber from FEL. Linear-rotary magnetic transfer arm (MTA) is placed in to FEL in order to transfer cantilevers and samples into the main chamber. The main chamber is evacuated with a 120 l/s diode ion pump and a liquid nitrogen cooled Titanium sublimation pump(TSP). A 150 l/s Varian Turbo molecular pump backed with a double stage rotary pump is used for pumping the FEL. This turbo pump is also used before starting the ion pump. The pressure of the system is measured by a nude ion gauge which is mounted on one of the ports in the preparation side of the chamber.

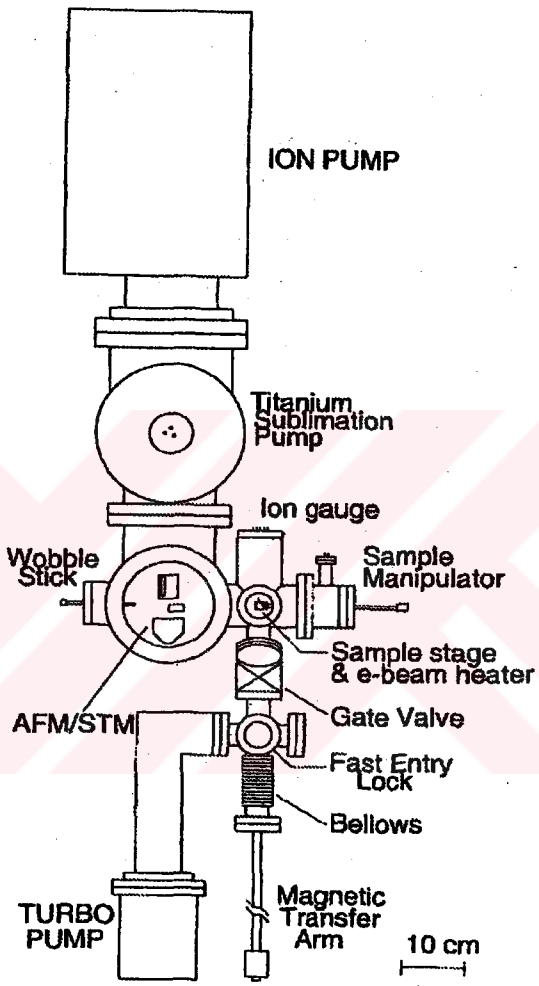

Figure 2.1: View of UHV system.[23]

The system is enclosed with detachable aluminum panels as a heat shield during the bake out, and three ceramic insulated heaters with total power of 2.2 KW are used to heat the system. A home-made temperature controller is used to keep the bake out temperature at the desired value of 155 °C. After the bake out all equipments in the chamber which has filament are degassed while the system is still hot .

2.1.1 Cantilever/Sample Transfer

Sample and cantilevers are transferred through FEL by using a magnetic transfer arm. After the FEL port is closed, the turbo molecular pump is run for about 1.5 hours, then the gate valve is opened and the sample or cantilever is transferred to the UHV chamber using the sample manipulator which is mounted onto push-pull/rotary-motion feedthrough. Then the sample and cantilever is transferred from the manipulator to the microscope stage or carousel using a pincer-grip wobble stick.

2.1.2 E-beam Sample Heater

The e-beam heater is built into the sample manipulator for sample cleaning. Top view of the e-beam heater is shown in Fig. 2.2. The filament is kept at -1200 V and the sample is grounded. The filament current,I_f , is adjusted to control the emission current,i_{em} , hence the heating power. The sample can be heated up to 1400 °C with this heater.

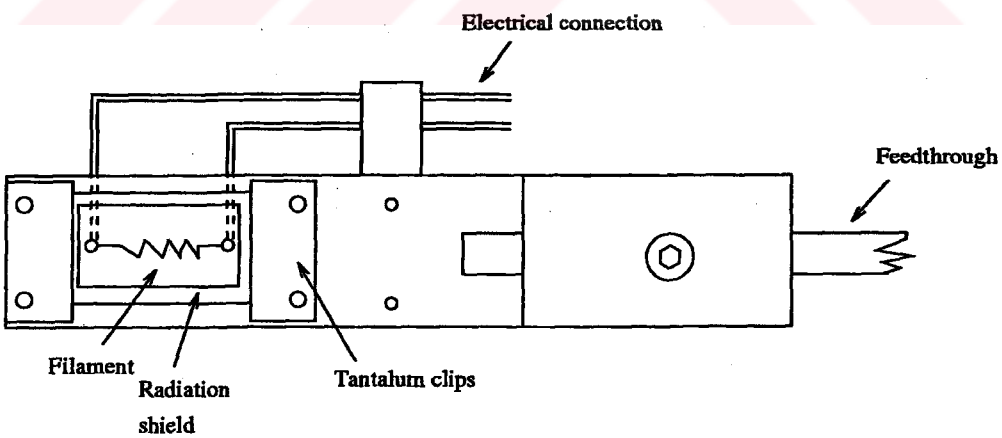

Figure 2.2: Top view of the e-beam heater.

2.1.3 Ge Evaporator

In order to grow Ge on Si surface, a simple-home made evaporator is constructed. A basket is made up of 0.5 mm diameter tungsten wire as a germanium source and mounted to 4-pin power feedthrough on 2.75" CF flange as shown in Fig. 2.3. Ge granules are put into the basket and the basket is attached to the power feedthrough pins by in-line barrel connectors. The evaporator is degassed for more than 24 hours while the sample is being degassed, in order to get rid of extra contaminants.

Figure 2.3: Germanium evaporator.[36]

2.2 The STM/nc-AFM Design

The microscope is mounted on a 8" special CF flange. This has two 20 pin instrumentation feedthroughs to bring electrical connections into UHV. The fiber feedthrough mounted on a 1.33" CF mini flange, which brings the fiber optic cable into UHV. There is a UHV linear motion feedthrough which is used to lock the base plate during sample and cantilever transfer to the microscope. In order to reduce the external vibrations, a single stage spring suspension system with eddy current damping is used. There are four springs mounted on adjustable collars to balance the microscope and four Sm- Co magnets are surrounded by copper plates attached to the microscope base for eddy- current damping. The microscope also contains two piezo coarse positioner; the sample slider and the fiber slider. The photograph of the STM/nc-AFM is shown in Fig. 2.4.

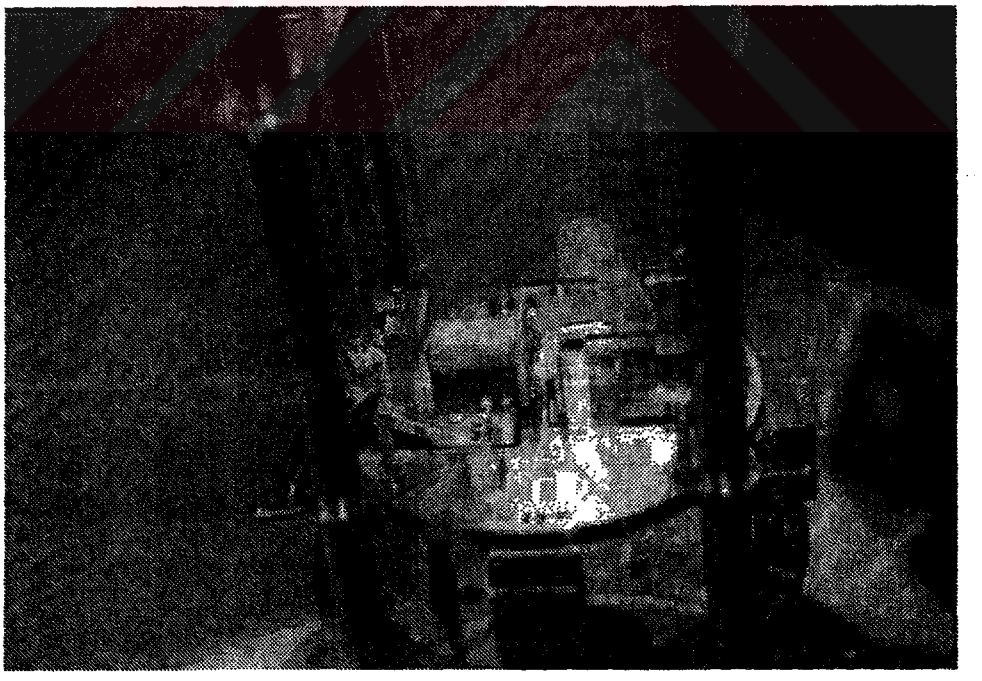

Figure 2.4: Close-up picture of the STM/nc-AFM.

2.2.1 The Sample Slider

The schematic view of a sample slider is shown in Fig. 2.5. The sample slider which performs the coarse approach of the sample towards the cantilever. The 3 dimentional scanning is performed by a tube piezo mounted on slider and the macor sample gluded on the end of piezo tube. The sample slider performs the coarse approach of the sample towards the cantilever, whereas the fine approach and scanning is achieved with the tube piezo.

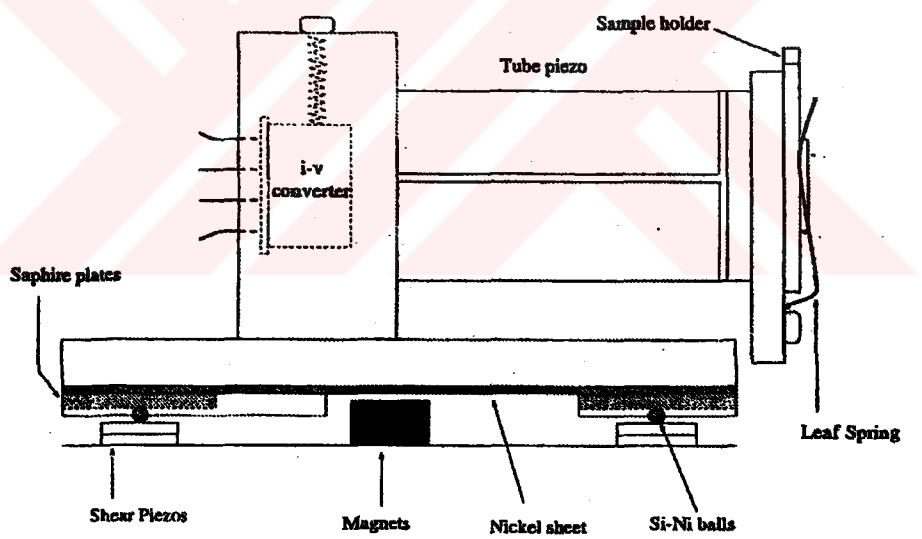

Figure 2.5: Schematic view of the sample slider. Taken from Ref.23

Coarse Approach

Under the slider, there are three set of cross polarized shear piezos: two front corners and one at the back. On top of each shear piezo set a small (1 mm diameter) Si_3N_4 ball is gluded. Sm- Co magnets mounted on the base plate under slider which pull the nickel plate at the bottom of the slider increase

the stiffness of the system. To move the slider, a voltage signal of the form $V \propto t^2$ is applied across the three shear piezos, which causes one electrode of the shear piezo moves with respect to the other electrode laterally and the inertia of the slider keeps it in its new position when the voltage is cut off and the piezo returns to its original size. Rapidly repeating the voltage pulses allows the slider to be moved in the desired direction at a rate of a few mm per minute. The slider is also able to move sideways by using the other set of which have polarization direction rotated by 90° with respect to other set. The slider can also be rotated clockwise and counterclockwise by applying voltage to the relevant piezos' electrodes. The coarse approach-slider's motion- is controlled by setting the frequency and voltage pulse duration through the computer program and then activating the different directions using joystick which is connected to the electronics. Figure 2.6 illustrates the principle of piezoelectric internal slider using shear piezos.

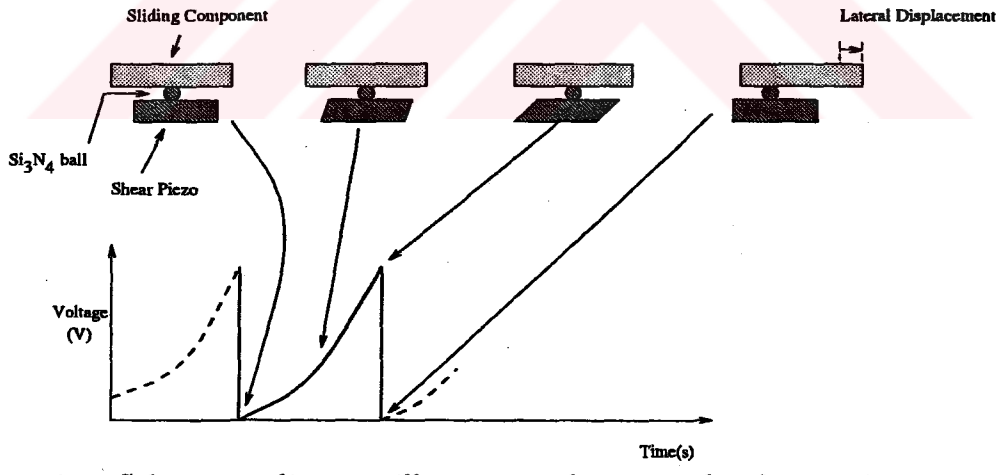

Figure 2.6: Schematic diagram illustrating the principle of piezoelectric internal slider using shear piezo.

Fine Approach and Scanning Mechanism

A single piezo tube serves as a sample scanner, the outer electrode of piezo tube is divided into four quadrants as shown in Figure 2.7. High voltages are

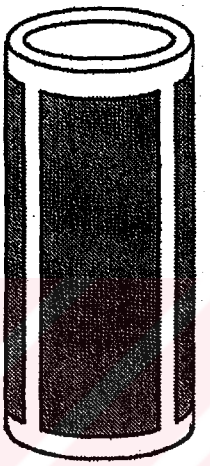

Figure 2.7: Tube piezo used in 3-dimentional sample scanner

applied to the quadrants to make the piezo expand or contract whereas the inner electrode is grounded. The sample is electrically connected by thin wire through the center of piezo tube to the Op- Amp which contains a 100 MΩ UHV compatible feedback resistor. This Op-Amp serves as a i- v convertor to measure tunnel current with a gain of 10^8 V/A. Fine approach of the sample to the tip is achieved by increasing the voltage applied to all four quadrants simultaneously until a tunnelling current is achieved. Gradually changing the applied voltages to the left and right quadrants allows the sample to be scanned across the tip. During the scan line, the feedback loop checks the measured current value and compare it with set current value, if there is a difference between the two then the voltage is applied to the quadrants is changed to move the sample so that the measured value matches the set value. At the end of each scan line the sample is returned to the start point, and the voltage applied to the top and bottom piezo quadrants is incrementally changed, so that the sample can be raster scanned. In STM feedback, the Z displacement of piezo is controlled by

the feedback circuit to keep the tunnelling current at a specified value and in AFM imaging the force gradient is kept at specified value by the feedback loop circuit.

2.2.2 The Cantilever Mount

A schematic view of the cantilever mount is shown in Fig. 2.8. The cantilever holder is kept in place by a leaf spring at the cantilever mount which is in turn fixed to the base plate. Electrical connection are made to the dither piezo to vibrate cantilever using an ac voltage and to the cantilever holder through the contact with the leaf spring in order to apply a dc bias voltage. The cantilever is electrically isolated from the dither piezo by a macor plate.

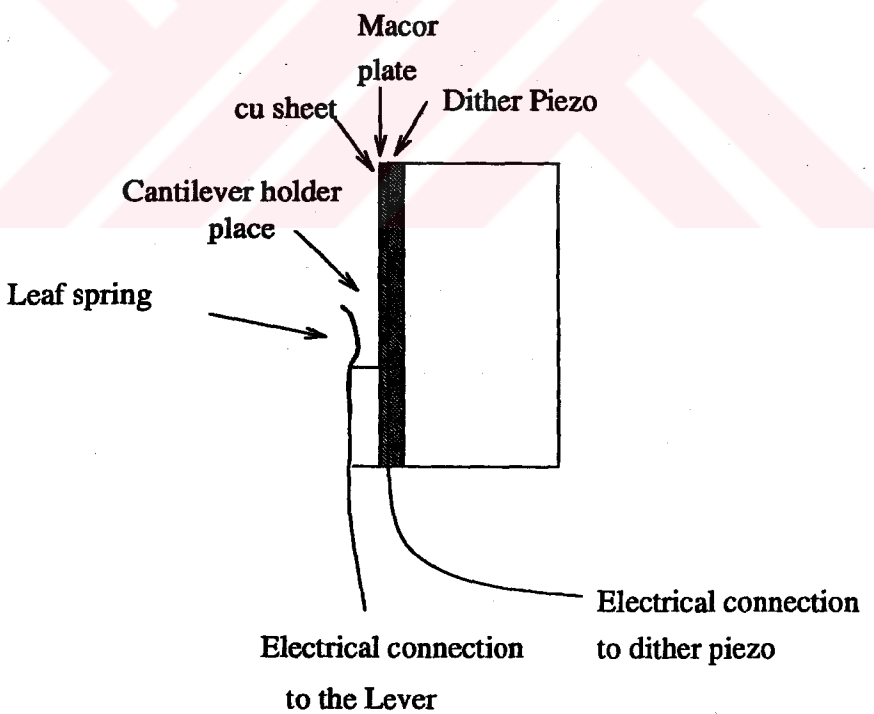

Figure 2.8: A schematic view of the cantilever mount.

2.2.3 Cantilever Preparation

Home-made tungsten cantilevers have been used in all the experiments. In most nc- AFM experiments, scientists prefer Si micro cantilever, but we wanted to have a metallic lever. Cantilever is one of the most important technical part of the microscope. Cantilever preparation is quite tricky and it requires extreme care. First, a 50 μm diameter tungsten wire is cut into ~1.5 cm pieces. The wire pieces are smashed between two polished tungsten- carbide pieces in order to create a mirrorlike surface at the back of the lever . The flattened wire pieces are polished in photographic film developer[42] to enhance the reflectivity. The flattened wire and graphite rod put into electrolyte and the wire is kept on positive potential between 20- 25 V, for less than a second. Then, the wires have to be bent 90°. The last step is electrochemical etching of the sharp tip. Bent tungsten wire is put into a solution of 2 M NaOH or (KOH) and is kept on a positive potential whereas the graphite rod serves as counter electrode. The electrochemical etching setup is shown in Figure 2.9.

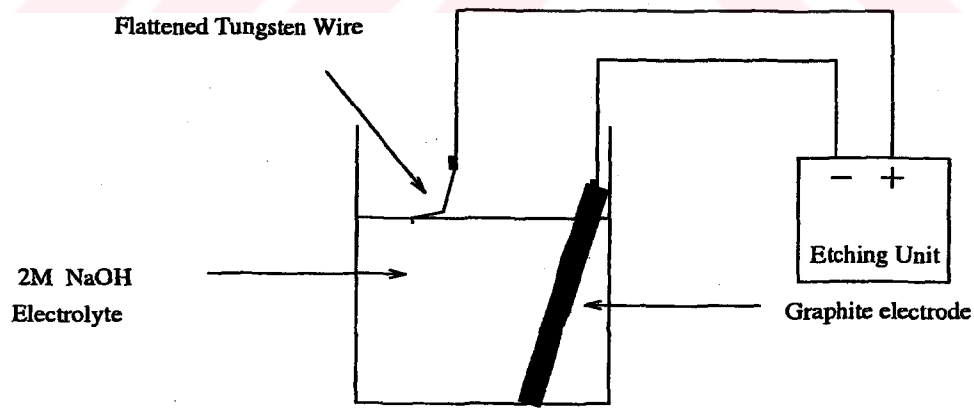

Figure 2.9: Electrochemical Etching Set up.

A home-made electronic circuit serves as a power supply and controller for etching process. Once the controller is turned on, the etching starts, the etching process takes place predominately on the surface of the solution. When the neck is thin enough the wire fractures due to its weight, the etching continues till

the wire is completely broken. The controller cuts the current as soon as the lower part of the wire falls off, creating a sharp tip. Tip should be cleaned with deionized water and pure ethanol (or methanol) in order to remove contaminates which come from the etchant. Once the tip is formed and cleaned, the levers are ready to be mounted on their holders. The cantilevers are glued on cantilever holder using a UHV compatible conductive epoxy.[41] After curing the epoxy, the levers are cleaned with Acetone and methanol in ultrasonic bath. In order to enhance the reflectivity of the levers further, the back part of cantilevers are gold coated. After the coating process, the levers are ready to use in STM/nc-AFM . Figure 2.10 shows a SEM image of prepared cantilever.

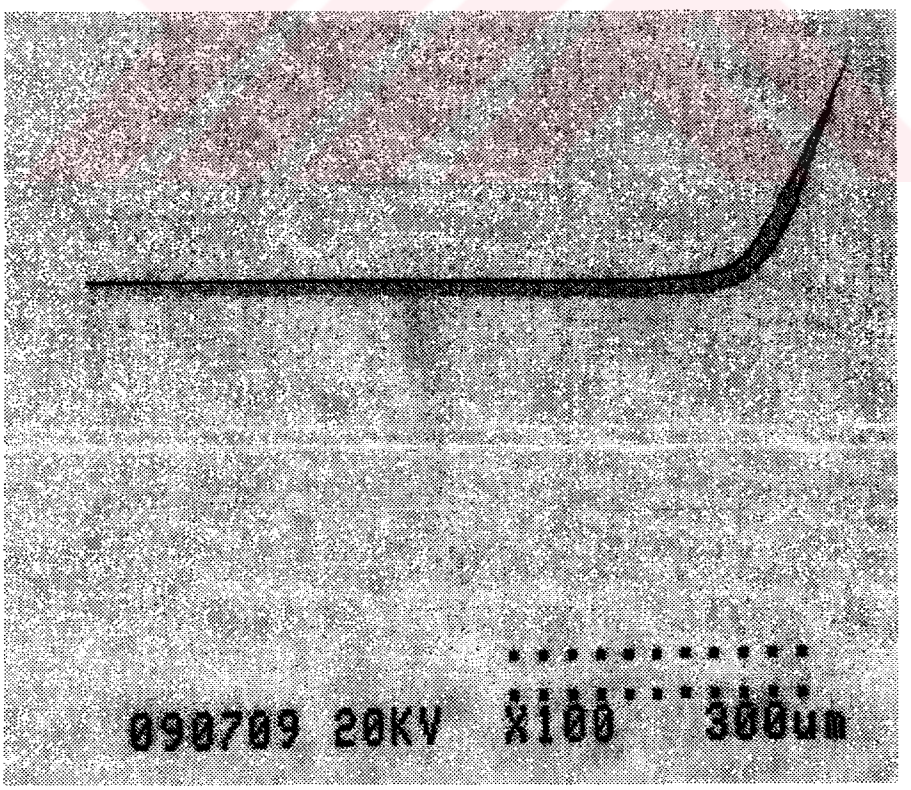

Figure 2.10: SEM image of a typical cantilever.

An atomically sharp tips needed to achieve the atomic resolution, . In fact, there is no any way to evaluate the quality of the lever unless it is used in microscope. Once the current is obtained, checking i- v curves and the stability of tunnelling current can give some idea about the quality of the tip. It is also possible, to sharpen the tip using bias voltage of $\mp$ 10 V for 3-4 lines scan.

2.2.4 Sample Preparation

Pieces of silicon, dimensions are (12×10× 0.5 mm), are cut from a Si(001) wafer. The samples undergo a series of etching and oxidizing steps developed by Ishizaka and Shiraki.[40] The silicon piece is first etched in a hydrofluoric acid solution (5% HF) for 30 seconds and then rinsed in deionized water, the etching removes any surface contaminations and impurities from the silicon. The sample is then oxidized in an ammonia and hydrogen peroxide solution ($1:1:3$ $H_2O_2 : NH_3 : H_2O$) for 30 seconds and then rinsed in deionized water again. This procedure is repeated 5 times and after each step the sample is dried by dry N_2 gas. The last step is oxidization of surface, therefore a thin oxide layer is formed on sample. The Si sample is dried and mounted on a sample holder, and transferred into the UHV chamber and onto the sample manipulator arm. The sample is degassed for at least 24 hours at 650 $°C$ using the e- beam heater. To remove the oxide layer properly, the sample is heated up to 900 $°C$ for two minutes, 1000 $°C$ for 2 minutes, 1100 $°C$ for 1 minutes and then cooled down very slowly. After the sample is cooled, it is transferred to the microscope.

2.2.5 Sample and Cantilever Holder

Sample holder is a 1 mm thick tantalum piece machined in rectangular shape of dimensions 20 × 15 mm^2 as shown in Fig. 2.11.

A rectangular hole is punched on which the sample is mounted for direct e-beam heating. Two tantalum leaf spring are spot- welded to the plate to fix the sample. A small hole at the upper part is used to hold the sample holder with magnetic transfer arm and wobble stick.

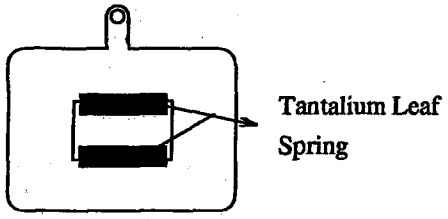

Figure 2.11: Schematic view of sample holder.

Cantilever holder is a stainless steel unique piece which is machined to form a stage for cantilever, the cantilever is gluded using a UHV compatible conductive epoxy[41]on the stage so that the apex of the cantilever is pointed to the sample. The schematic view of the cantilever holder is shown in Fig. 2.12.

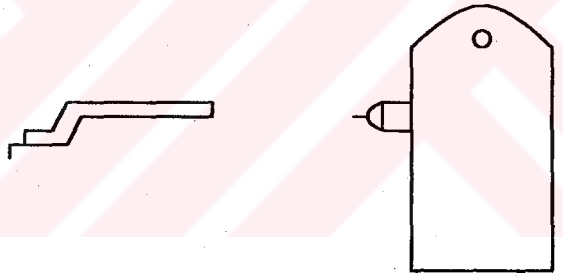

Figure 2.12: Schematic view of cantilever holder.

In earlier experiments, the cantilever holder which had many gluded parts were used. We designed a single piece cantilever holder to reduce the complication. All the experiments in this thesis carried out by the new cantilever holder.

2.2.6 Force Sensing Technique: Interferometry

A fiber optic interferometer is used to detect the deflection of the cantilever. Our optical fiber interferometer is shown in Figure 2.13.

The interferometer design is similar to that used by Rugar *et al.*.[5,43] We use a 3.8 mW semiconductor laser diode with a wavelength of 1310 nm. All the fiber

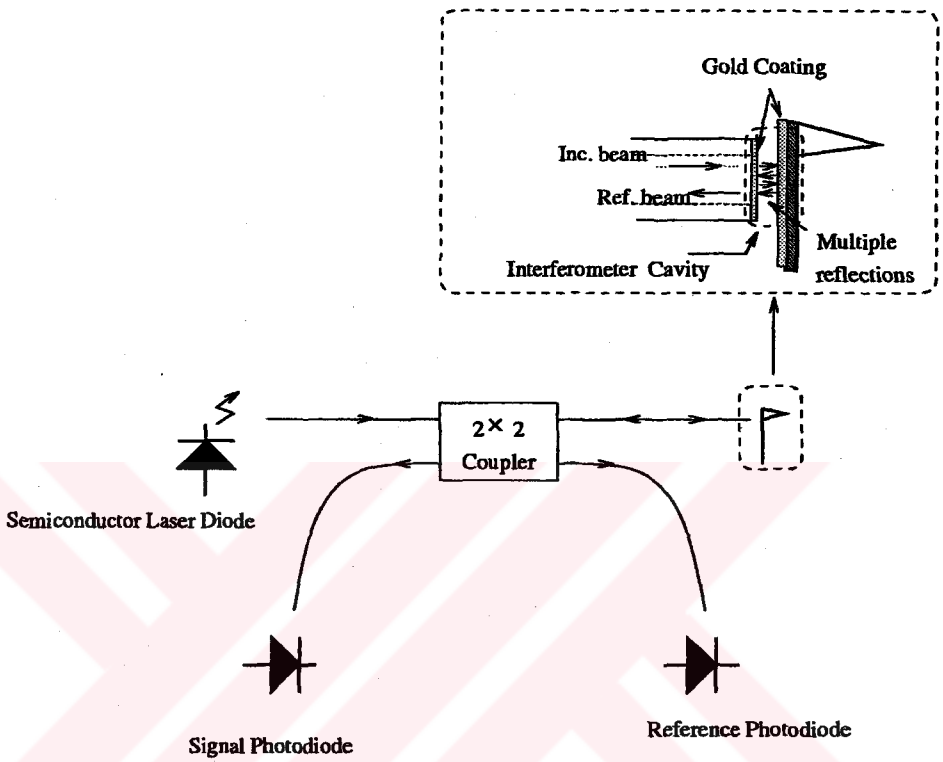

Figure 2.13: Schematic diagram of the optical system.

optic cables are single mode and FC/APC connectors are used to connectorise the cables.

Light from a laser diode is split by a (50-50) coupler and half of the beam goes to the reference photodiode. The other half goes to the end of the fiber. The end of the fiber is gold coated, therefore some part of the light is reflected back in to the fiber. The rest impinges on the back of the cantilever and reflected from it. Therefore we obtain multiple reflections which form a Fabry- Pèrot interferometer cavity between the end of the fiber and the back of the cantilever. This causes radical enhancement in the sensitivity. A typical interference pattern is shown in Figure 2.14 , the laser power has been set to 2.3 mW and a visibility of 0.257 was obtained.

The fiber end is mounted on a piezo tube which is used to adjust the fine position of fiber at the back of the cantilever. The light which is coupled back into the

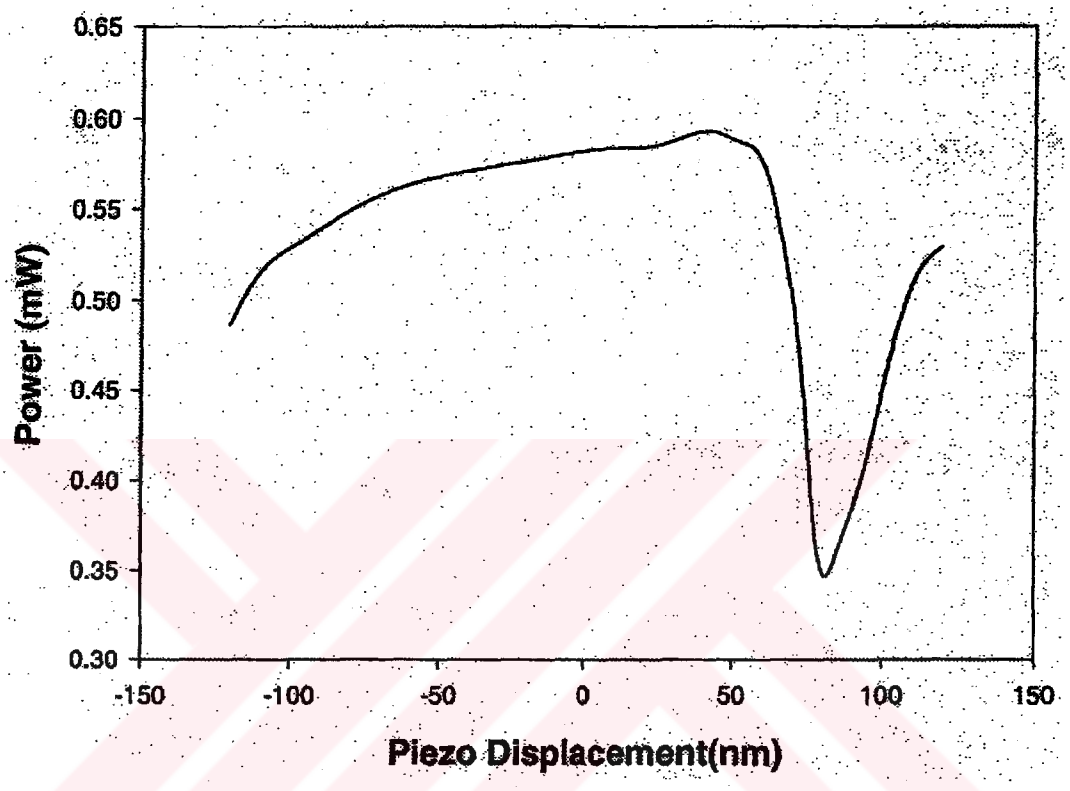

Figure 2.14: A typical interference pattern.

fiber is split again by the coupler and half of it goes to the signal photodiode. The interferometer response can be modelled as a simple two-component interference, if multiple reflections in the interferometer cavity is ignored. The current from the signal photodiode is given by

$$i = i_{\circ}[1 - V\cos(4\pi d/\lambda)] \tag{2.1}$$

Where λ is the current laser wavelength and d is the fiber-to-cantilever distance. The quantities V and $i_{\circ}$ correspond to the fringe visibility and the average current, respectively, and are given by $V = (i_{max} - i_{min})/(i_{max} + i_{min})$ and $i_{\circ} = (i_{max} + i_{min})/2$, where i_{max} and i_{min} are the currents corresponding to maximum constructive and destructive interference, respectively. The average

current and visibility can also be expressed by different parameters[5] which are as follows:

$$i_o = P_{av}S = (P_r + P_s)S \tag{2.2}$$

$$V = 2\sqrt{P_r P_s}/(P_r + P_s) \tag{2.3}$$

Where P_r, P_s, P_o ,P_{av} and S are reference and signal power at the photodiode, laser out put power, average power incident on the photodetector and the photodiode sensitivity, respectively.
In the presence of multiple reflection photodiode current can be expressed on[23]

$$i = i_o[1 - VF(4\pi d/\lambda)] \tag{2.4}$$

Where F is a periodic function of d. The multiple reflections enhances the sensitivity. The most sensitive operation is where the phases of the two reflected components are in quadrature, or $d = \frac{\lambda}{8}, \frac{3\lambda}{8}, \frac{5\lambda}{8}, ...$ At quadrature, changes in photocurrent, Δi response for small changes in distance, Δd, and wavelength, $\Delta\lambda$, is given by

$$\frac{\Delta i}{i_o} = 4\pi V\frac{\Delta d}{\lambda} - 4\pi dV\frac{\Delta\lambda}{\lambda^2} \tag{2.5}$$

The *shot noise* level of the system is the lower limit to sensitivity of the interferometer which is

$$d_{shot} = \frac{\lambda}{2\pi Vm}\sqrt{\frac{eB}{2SP_{av}}} \tag{2.6}$$

where λ is the laser wavelength, e is the electronic charge, B is the detection bandwidth. m is the ratio of the slope of the interference pattern and the slope of ordinary Michelson fiber optic interferometer system.

2.2.7 Fiber Slider

A fiber slider is used to position the fiber at any point at the back of the cantilever. The fiber slider consists of two separate sliders which can move and rotate in a plane. Figure 2.15 shows a schematic view of the fiber slider. Similar to

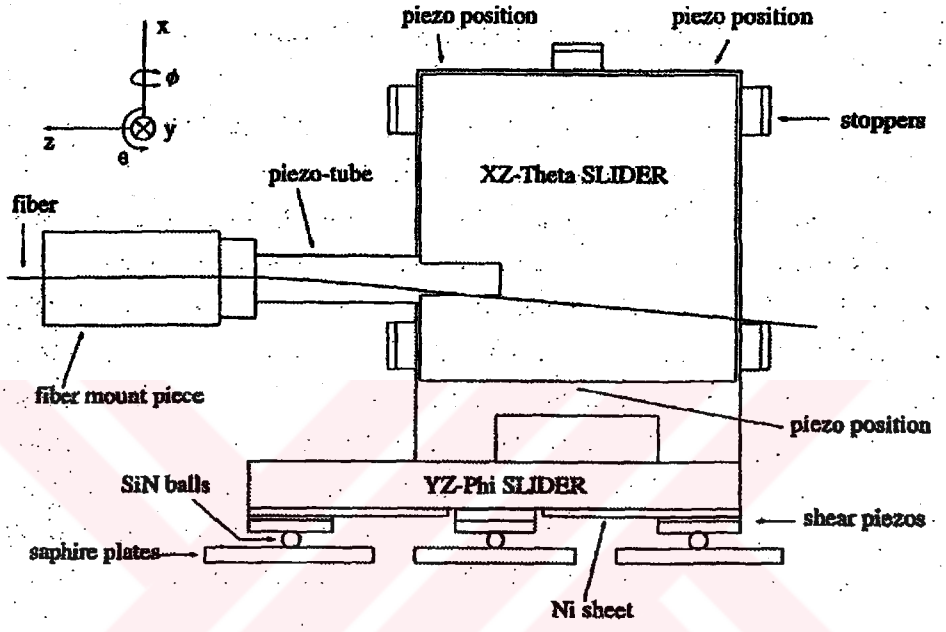

Figure 2.15: Schematic view of the fiber slider.[23]

sample slider, the $YZ\phi$ slider has Si_3N_4 small balls glued onto the shear piezos mounted under the body . The fiber slider can be moved in the same way as the sample slider. The second slider is mounted vertically on top of the first slider, and can move forward, backward, up and down and can be rotated clockwise and counterclockwise in the vertical plane in which the slider is mounted. This arrangement provides accurately positioning the fiber behind the lever. The fiber itself is mounted on a tube piezo, which for fine positioning of the fiber and to keep the instrument at quadrature point.

2.2.8 Electronics and Computer Control System

The STM/AFM is controlled by a personal computer through an Electronic control unit. Schematic view of electronics is shown in Figure 2.16. The control electronics consists of eight PCB cards. There is a power supply card which

supplies 5 V, ±8 V, ±15 V, ±220 V and 300 V to the other cards, a HV amplifier card to supply voltages to the sample scanner piezo quadrants, a card to supply the voltage pulses to the sliders' shear piezos, a photodetector card that contains the laser diode, the coupler and the two photodetectors, an analogue to digital converter card, a digital to analogue converter card which supplies various voltages under computer control, and the feedback control which regulates the tip sample separation. All the functions of electronics are controlled through the software is written in Borland Pascal, and has been specially developed to control the microscope. The program performs automatic sample approach, imaging , force- distance spectroscopy as well as various image processing algorithms, in order to analyse the data. Coarse approach of the sample to the tip is controlled the setting the frequency and duration of the voltage pulses to the shear piezos and using a joystick connected to the electronics to select the direction of motion. The fine approach of the sample to the tip is automatically controlled by computer. Before automatic approach is started, the feedback loop gain is usually set to its maximum value, the number of voltage pulses per cycle is set so that the slider moves forward a shorter distance than the maximum piezo extension. This prevents crashing the tip into the sample during approach. The approach involves the following steps: the tube piezo is extended until it reaches its full extension or a tunnelling current is found, if no tunnelling current is found the tube piezo is fully retracted, a number of steps are made by slider and then the piezo is extended again, this procedure is repeated until a tunnelling current is found. If the AFM mode is being used, the feedback signal comes from lock-in amplifier, which measure the lever vibration amplitude, and the approach stops when a set force gradient is found.

The program can record interference patterns and display them on screen, and the patterns can be saved. The details of the maximum and minimum power, the visibility, and the power at the signal and reference photodiodes are displayed on screen. The slope of the interference pattern is also displayed. The program can also be set to keep the interferometer at the quadrature point. To do this the computer records an interference pattern and calculates the quadrature point.

The fiber piezo is used to keep the fiber at the position which keeps the laser power at the same value as at the measured quadrature point. For imaging, numbers of parameter need to be set. The tip bias voltage, set tunnelling current and feedback loop gain can all be set via the software, the position of scan area can be controlled by using offset voltages. The pixel size of the images can be set manually in a 128×128, 256×256 or 512×512 matrix form and a automatic routine is used to record images. The software allows up to 5 channel to be recorded as an image from each channel, the gain for each channel can be set separately. If the scan parameters that are set are to be kept constant for number of scans, there is also an option that makes the program check the tip-sample position whether it is within tunnelling range or not, if the sample is too close or too far from the tip then an appropriate numbers of step is made by the slider to bring the sample back or close to a point where only a small voltage is applied to the tube piezo. Keeping the voltage applied to the tube piezo close to 0 V reduced the amount of piezo creep. Cross section of the images also can be plotted which gives better idea about surface corrugation. The $I - V$ curves can also be acquired.

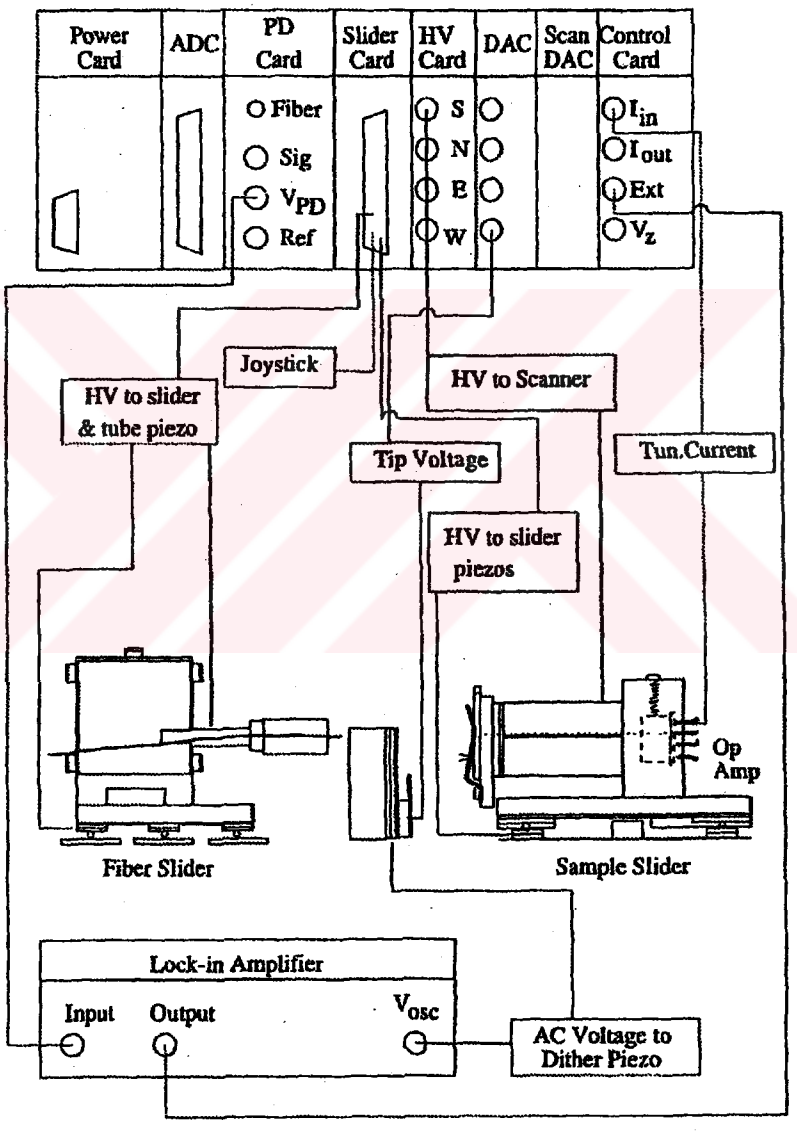

Figure 2.16: Schematic view of the electronics. Taken from Ref. 23

Chapter 3

Si(001) Surface and Ge/Si(001)

3.1 Si(001) Surface

The exceptional electronic and structural properties of silicon, offer special attention, because of its importance in the microelectronics industry and nanoscale research. When a Si crystal cut along the (001) plane, each surface atom is left with two dangling bonds. The surface reconstructs to form rows of *dimerized atoms*, yielding a (2×1) unit cell, the driving force for reconstruction is the reduction in the number of dangling bonds from two to one. Schematic view of the Si(001) surface is shown in Fig. 3.1. This rearrangement of surface, reduce the surface free energy and the surface configuration is more stable. Experimental efforts in order to confirm this rearrangement started by Schlier *et al.*[27] in 1959, they used Low Energy Electron Diffraction (LEED) technique to observe the Si(001) structure, by this method they proposed (2×1) reconstructed surface, but this proposition of surface atom pairs (dimers) was not easily accepted, because the LEED study of Schlier *et al.* yielded higher order diffraction spots as well!. For many years after the first LEED study, although dimer rows in surface structure were confirmed by several models, still there were some weak points in the model because of important inconsistency in the LEED studies by different groups. The invention of Scanning Tunnelling Microscope and the first result from the investigation of the reconstructed Si(001) surface on the atomic scale

by Tromp *et al.*[28] has verified the dimer model.

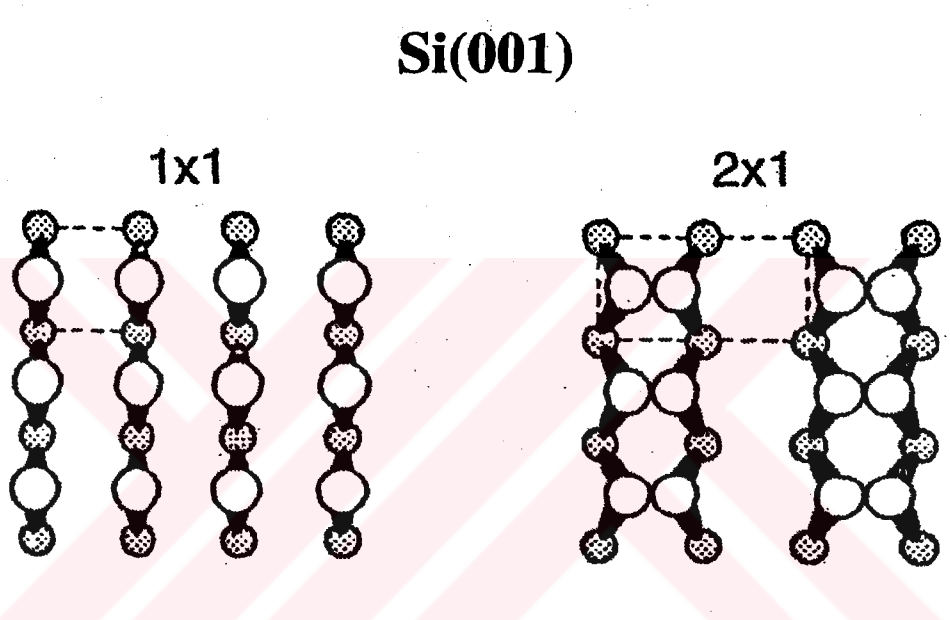

Figure 3.1: Schematic view of the Si(001) reconstructed surface. Taken from Ref.39

In addition to dimer row structure of Si(001) surface, steps and vacancies on Si(001) surface form as a result of complex behavior that depends on many factors like miscut angle, annealing, growth conditions, and surface stress. Step is a boundary between two terraces. Because of the tetragonal bond structure of silicon, the dimers on two terraces which are separated by a monoatomic step, the dimerization direction is perpendicular to each other. The dimer rows on the upper terrace which form parallel to the step edge, is called type A, labelled S_A and the dimer rows which aligned perpendicular to its edge is called type B and is labelled, S_B. Double step also forms on Si(001)rather than monoatomic step and the direction of dimers do not change through such kind of steps, therefore the dimer rows are in the same direction in the upper and lower terraces of the

step. These steps, depending on their type are called D_A and D_B. Top view of the different dimerization directions are shown in Fig. 3.2 schematically.

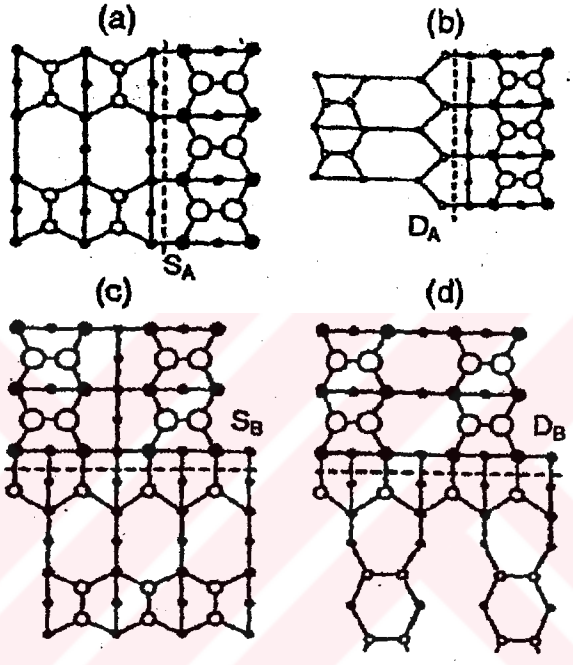

Figure 3.2: (a)-(d) Top views of S_A, D_A, S_B and D_B respectively. The dimerization direction of the topmost atoms is along the [110] direction. The dashed lines indicate the step positions. Open circles denote atoms with dangling bonds. Larger circles are used for upper-terrace atom. Taken from Ref.39

3.2 Ge/Si(001) System

There is a lot of interest in growing semiconductor clusters or quantum dots on semiconductors. Such clusters are useful in a variety of new applications such as quantum dots for single electron transistors, memory devices and optoelectronic devices. There are several semiconductor nano cluster examples, like InP/GaAs, InAs/GaAs.[30] Germanium on silicon is a system which have been studied by

many groups[31–34] using STM, but to the best of my knowledge, there is no study of investigation of epitaxial growth of Ge on Si(001) by using nc-AFM. We have attempted to study this system by using our low oscillation amplitude nc-AFM technique. In Ge/Si(001) system 4% lattice mismatch between Si and Ge gives rise to spontaneous cluster formation. Ge growth is a non-equilibrium process.The system will try to relax back to equilibrium by forming a condensed phase of many small 2D, 3D islands or through adsorption of ad-atoms, consider disposition of a small of a monolayer on a substrate. Randomly arriving ad-atoms make random walks on the surface and they can either meet each other to form islands or walk into steps. Figure 3.3. shows the Terrace- Step- Kink model of the atomic mechanisms of the crystal growth.

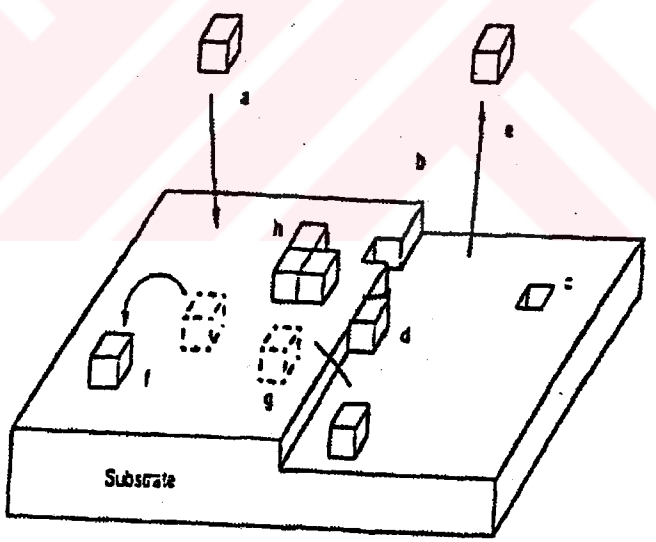

Figure 3.3: Atomic mechanism of crystal growth, the Terrace-Step-Kink model. Arriving atoms(a), land on the surface which contains terraces, steps (b), vacancies (c) and kinks (d), Atoms can evaporate (e), move on the terrace (f), cross over the step (g), nucleate new islands (h) or become incorporated in to steps. Taken from Ref. 35

For many systems and certainly Ge/Si(001), single ad-atoms are the most mobile species and two atoms which represent a dimer, form a stable cluster, which will have much lower mobility than the single ad-atom. Even a dimer is not a

stable cluster, however its mobility will in general be greatly reduced. Therefore, once an ad-atom is incorporated into any cluster, its random walk is stopped and it will not be able to hop to a substrate step, as long as the substrate temperature is low enough, atoms are not re-evaporated from clusters. This competition between island nucleation and the incorporation at substrate steps leads to depleted region,like Stranski-Krastanov mode behavior (layer-by-layer growth followed by three-dimensional island formation) or denuded zone in the spatial distribution of island near steps. A denuded zone is therefore a striped area along the step in which the island density is much lower than that the far from the step. It is formed because the ad-atoms landing near a step are able to migrate to the step in without colliding with each other to form islands.

Chapter 4

Results and Discussion

After sample preparation in the UHV, sample is loaded in STM/nc-AFM for imaging and force-distance spectroscopy. The sample is scanned with respect to the tip while the feedback run in STM mode. During scan, four channels are recorded simultaneously. First channel is recorded the oscillation amplitude of the lever, measured by the lock- in amplifier, second channel is recorded V_z, STM topography, third channel is the deflection of the cantilever, for dc-force, and the forth one is the phase output of the lock-in amplifier, for loss measurement. The reverse scan of the lock-in amplitude is also recorded to check the reproducibility of forward and backward scan lines.

We also recorded force-distance (F-d) spectroscopy to investigate tip-surface interaction quantitatively. When the tip is in tunnelling the feedback is suspended and the sample is pulled back by a specified distance. Then it is advanced toward the tip while recording tunnelling current, force gradient, dc-force (cantilever deflection) and phase.

Our microscope relies on vibrating a stiff lever at sub-Ångstrom oscillation amplitude and the changes in amplitude due to the tip-surface interaction are measured. In the following section, theory of small amplitude nc-AFM which is worth to know in order to understand the interpretation of our experimental results will be described.

4.1 Theory of Small Amplitude nc-AFM

We used a simple mass and spring model to analyse our results. The cantilever base is dithered by a piezo at frequency,ω , with an oscillation amplitude,A_d. As shown in Figure 4.1.

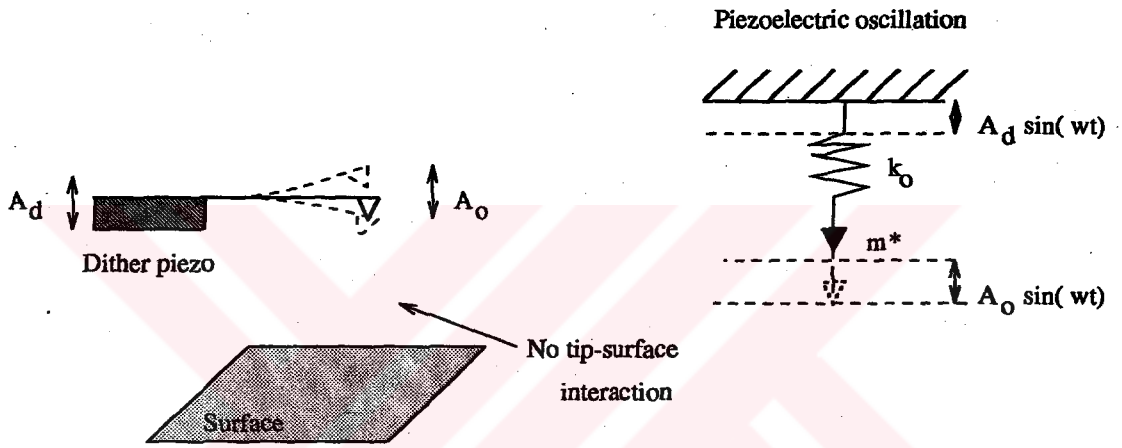

Figure 4.1: Illustration of the model. Tip-surface interaction is ignored. Right scheme shows mass-spring model.

Therefore if we assume the cantilever obeys the Hooke's law: $F = k_o z$ and the equation of motion can be written as:

$$m^* \ddot{z} + k_o z = F_o \sin(\omega t) \tag{4.1}$$

Where m^* is the effective mass and k_o is the stiffness of the lever, respectively, and F_o is the applied force to the cantilever via dithering the piezoelectric element which can be express on $F_o = k_o A_d$. The equation of motion has a solution of the form $z = A_o \sin(\omega t)$, if the force associated with A_d is taken in to account, the free oscillation amplitude, will be:

$$A_o = \frac{k_o A_d}{m^*(\omega_o^2 - \omega^2)} = \frac{k_o A_d}{m^* \omega_o^2 (1 - \frac{\omega^2}{\omega_o^2})} = \frac{A_d}{(1 - \frac{\omega^2}{\omega_o^2})} \tag{4.2}$$

where $\omega_o = \sqrt{\frac{k}{m^*}}$ is the resonance frequency of the lever. In our experiments the driven oscillation frequency is far below the resonance frequency ($\omega \ll \omega_o$),

therefore $A_o \simeq A_d$.

Now we consider a more realistic model. As before, The cantilever is again modelled as the mass-spring system, but now a finite tip-surface interaction is also included. As shown in Figure 4.2.

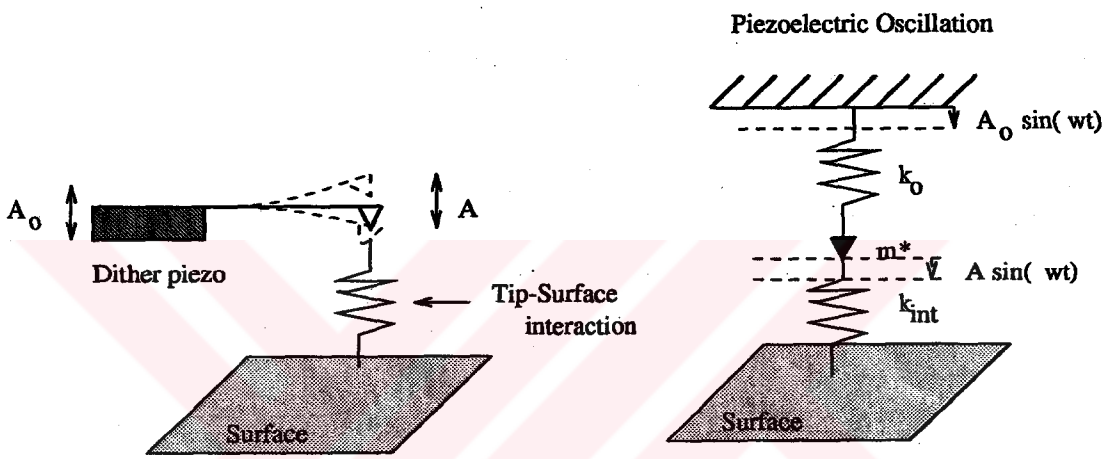

Figure 4.2: Illustration of the model. Tip-surface interaction is considered. Right scheme shows the mass-spring model.

Like the first approach, the dither piezo is used to create free oscillation displacement, A_0, but in the presence of tip-surface interaction at the proximity of the surface the tip oscillation amplitude ,A ,is measured. We can write down a force balance for the system:

$$-k_0(A_0 - A)\sin(\omega t) = k_{int} A \sin(\omega t) \tag{4.3}$$

Therefore the interaction stiffness can be extracted as:

$$k_{int} = -\frac{dF_{int}}{dz} = k_0(\frac{A_0}{A} - 1) \tag{4.4}$$

The above equation shows that by using the small amplitude method, force gradient is measured rather than force.

4.2 Si(001)(2×1)

As mentioned in previous chapter, Si(001) undergoes a reconstruction feature. In summary, there are two unsaturated bonds per surface atom on the bulk terminated Si(001) surface. This, in fact, explains why the (001) surface is a reactive surface. During reconstruction each atom on the surface is bonded with its neighbor by using one of its unsaturated dangling bonds forming a "dimer" to minimize the total energy. Since Si has tetrahedral bonds, dimers on terraces which are separated by monoatomic steps are rotated 90° with respect to each other and the process create different types of steps on (001) surface.

In order to perform an experiment on the Si(001) surfaces the Si(001) samples were prepared as mentioned in section 2.2.5. After flashing the sample at high temperature, the sample is cooled down to the room temperature and then transferred to the microscope. After aligning the fiber at the back of the lever for the highest sensitivity, the sample is approached had to get tunnelling current.

Figure 4.3 shows STM topography and force gradient recorded simultaneously. The oscillation frequency and oscillation amplitude were set to 7.95 kHz, which is far below resonance frequency of the lever and 2.3 Å, respectively. The tip bias voltage and tunnel current were set to -1.5 V and 1 nA, respectively. The STM topography and the force gradient do not show exactly the same features, but in both images, the dimer rows and defects are resolved. The contaminations on surface are also shown as bright spots. The force corrugation (black to white scale) is 3.44 N/m.

Figure 4.4 shows another scan of different area of the same sample with a smaller tunnelling current 0.5 nA. In both images dimer rows and defects are resolved. There are some feature are resolved in the STM topography while they are not shown in force gradient image, perhaps it illustrates different tip-surface interaction nature between the STM and the force gradient during imaging. The force corrugation (black to white scale) is 2.34 N/m.

Figure 4.5 shows a set of scan, in STM topography and force gradient images the dimer rows are resolved, dc-force image is noisier, but dimer arrangement still

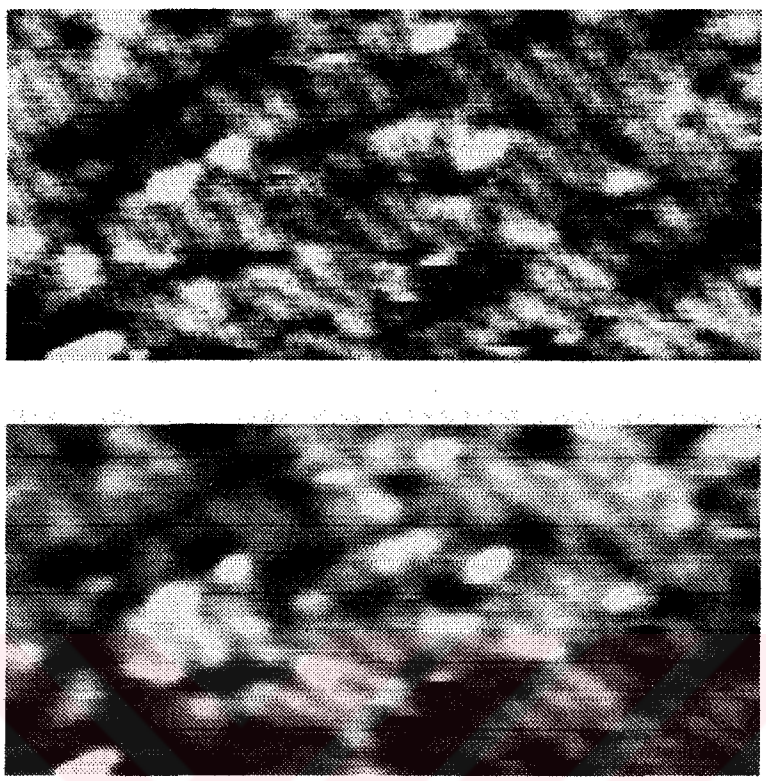

Figure 4.3: Simultaneous STM(top) and force gradient(bottom) images of Si(100) (2×1) - Image size is 154 ×77 Å^2. V_{bias}= -1.5 V, I_t= 1 nA, k_o= 157 N/m and A_o= 2.3 Å. Black shows more negative value in the force gradient image.

can be seen. The bottom part of images are slightly disordered due to creep of the sample scanner.

4.3 Force-Distance Spectroscopy on Si(001)

The force distance spectroscopy were also performed on Si(001)-(2×1). The measurement started when the tip was in tunnelling. Measurement were made by retracting the sample by a specified distance from the tip, and then advancing toward the tip until a set tunnel current was reached. The tunnel current, lever deflection and force gradient were recorded simultaneously during the approach and retraction.

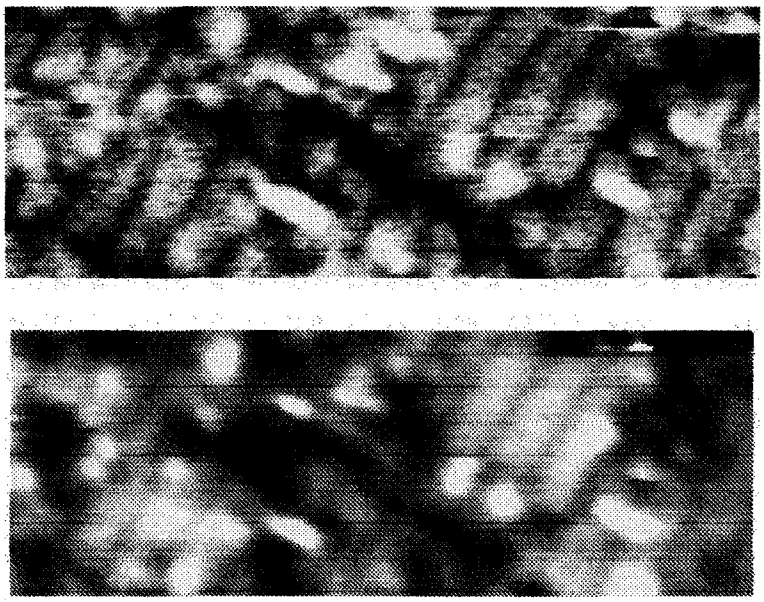

Figure 4.4: Simultaneous STM(top) and force gradient(bottom) images of Si(100) (2×1) - Image size is 110 ×38 Å^2. V_{bias}= -1.5 V, I_t= 0.5 nA, k_o= 157 N/m and A_o= 2.4 Å. Black shows more negative value in the force gradient image.

Figure 4.6 shows a force-distance spectroscopy curve. The oscillation amplitude of the lever was 2.4 Å. The interaction stiffness reaches -28 N/m, which is the maximum attractive interaction and then turns to positive interaction stiffness. It should be noted that the length scale of the interaction is about 12 Å. Therefore it can be illustrated that the long range interactions like vdW and electrostatic are responsible rather than short range interaction like covalent force. Almost reversible changes in force gradient curve on approach and retraction represent a small amount of energy dissipation during tip-surface interaction.

Figure 4.7 shows another force-distance measurement for one approach of the sample to the tip. The free oscillation amplitude is 0.25 Å. Force gradient becomes negative before turning up and becomes positive as the sample approached further toward the tip . The maximum attractive interaction is -32 N/m, and the length scale is about 5 Å.

Comparison between the results suggest that using a low amplitude oscillation amplitude can open an opportunity to measure short range interaction.

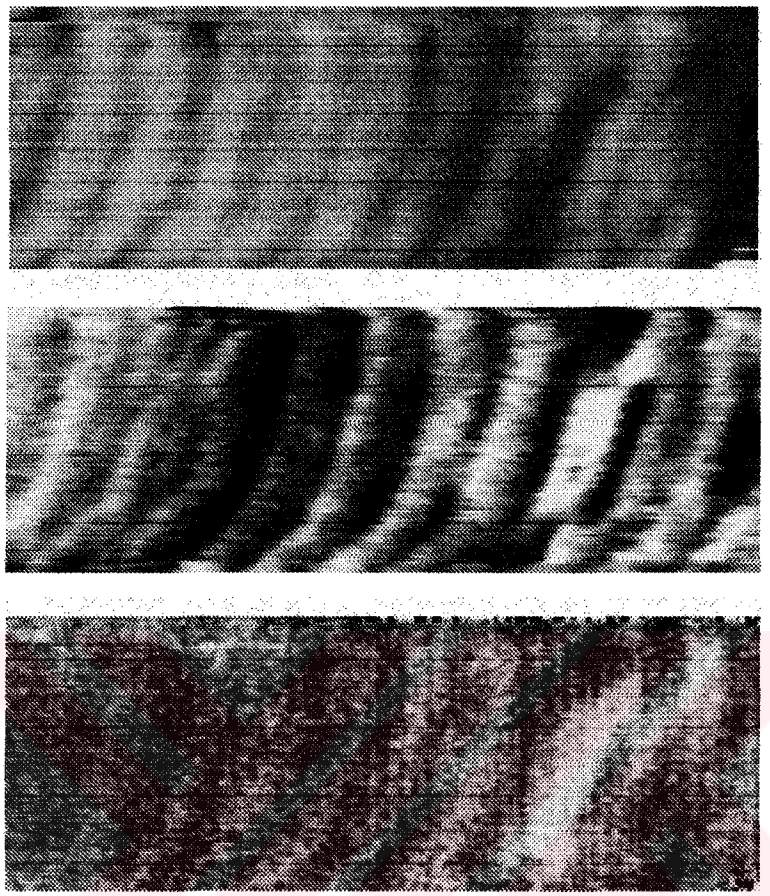

Figure 4.5: Simultaneous STM(top), force gradient(middle) and dc-force(bottom) images of Si(100) (2×1) - Image size is 110 ×40 Å^2. V_{bias}= 1.5 V, I_t= 1 nA, K_o= 160 N/m and A_o= 0.25 Å. Black shows more negative value in the force gradient image.

4.4 Ge Epitaxial Growth on Si(001)

In the next phase of experiments, germanium have been epitaxially grown on clean Si(001)substrates. Simple home-made thermal evaporator is used to grow the epitaxial layers as described in section 2.2.3. The evaporator is degassed for more than 24 hours at the temperature near to the evaporation temperature, to get rid of extra contaminations, while the sample is degassing. After flashing the sample at high temperature, the sample is left to cool down to the room temperature. In order to grow Ge, the sample was first positioned facing back so

that it was not exposed. The evaporators were activated at suitable power until the pressure, in the chamber is stabilized. After stabilization of pressure the sample was faced to the source. The surface was exposed for the desired coverage and then turned back to the original position and the evaporator's power were slowly turned down. At the earlier step of the experiment we tried to calibrate the rate of deposition of Ge on substrate. In our experiment the coverage is measured by counting the area of the Ge dimers on the surface away from the steps and divided it by the total area. We tried to gain some idea for the exposure parameter from the previous works have done by Oral,[36] because of different specifications in our systems, we couldn't obtain the same result. However, the germanium source current was set to 7.0 A_{rms} and Ge was deposited for 45 second on the sample. The pressure rise due to evaporation was $\Delta p \sim 1.8 \times 10^{-9}$ mbar. During growth, the substrate temperature was kept at room temperature to decrease the diffusion length and mobility of adatoms, because we aimed to investigate island formation on substrate rather than step slow growth. After expose the surface, the sample is transferred to the microscope. We used STM/nc-AFM with low oscillation amplitude to investigate Ge growth on Si surface. Stiff Tungsten levers were used. The resonance frequency was found to be 17.9 kHz and the lever was set to vibrate at 6.240 kHz .

Figure 4.8 shows simultaneous STM topography and force gradient images of $\sim$ 0.4 ML Ge on Si(001), the faintly Ge dimers can be seen in STM topograph but the contaminations on surface make the images, unclear, perhaps because of inappropriate degassing of Ge granules and evaporator. The lock-in signal is very noisy so that in force gradient image there is no contrast.

Figure 4.9 shows another simultaneous STM topography and force gradient images of $\sim$ 0.2 ML Ge, in both images a few debris Ge dimer like can be seen but the density of contaminations on surface is high.

Figure 4.10 is also shows images obtained from another run and reveal reproducible features, in both STM topograph and force gradient images. The rows are improperly stretched, perhaps because of bad quality of the tip or thermal drift.

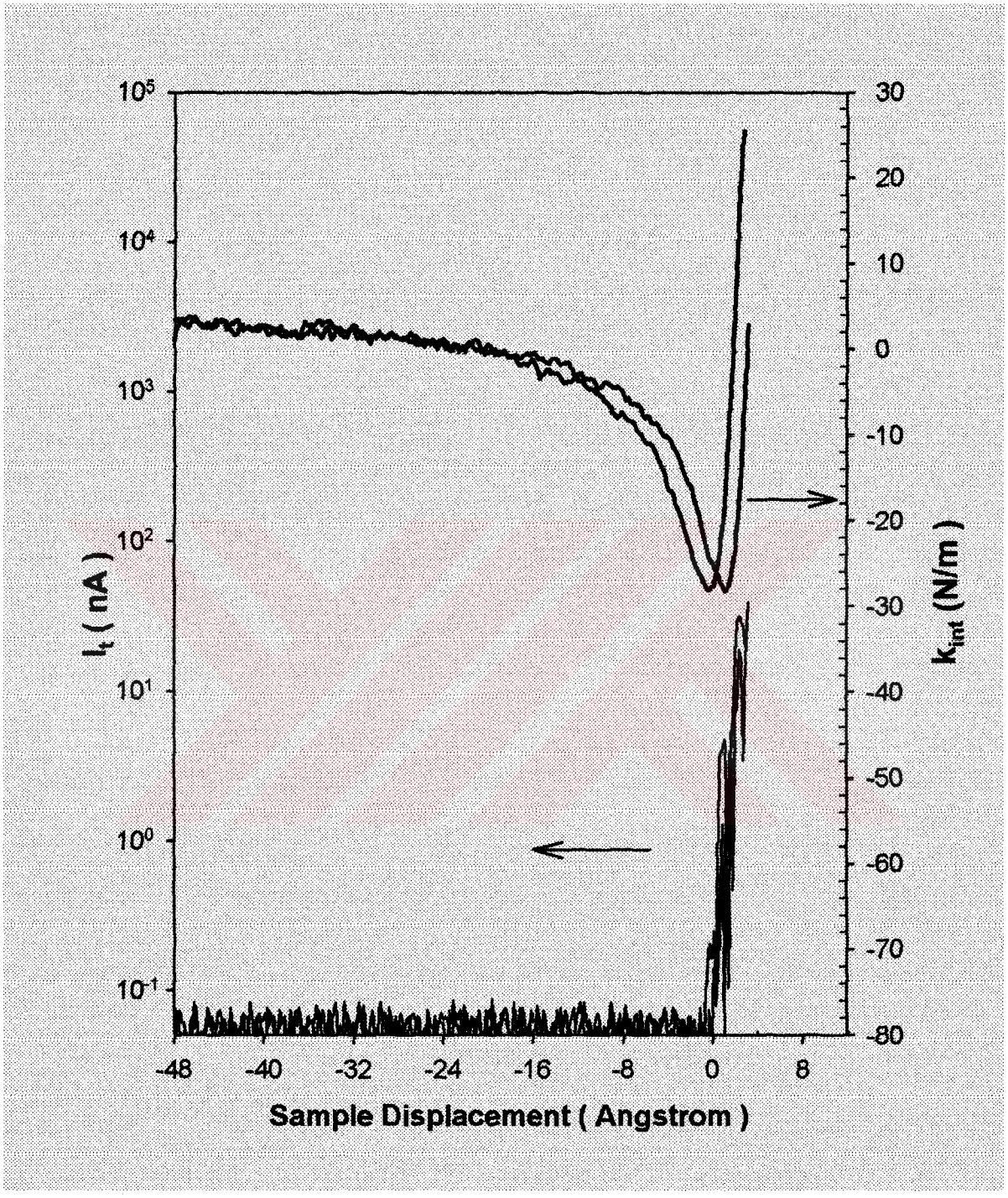

Figure 4.6: *F-d* spectroscopy curve, shows simultaneously tunnel current and force gradient measurement. k_o=157 N/m and A_o= 2.4 Å.

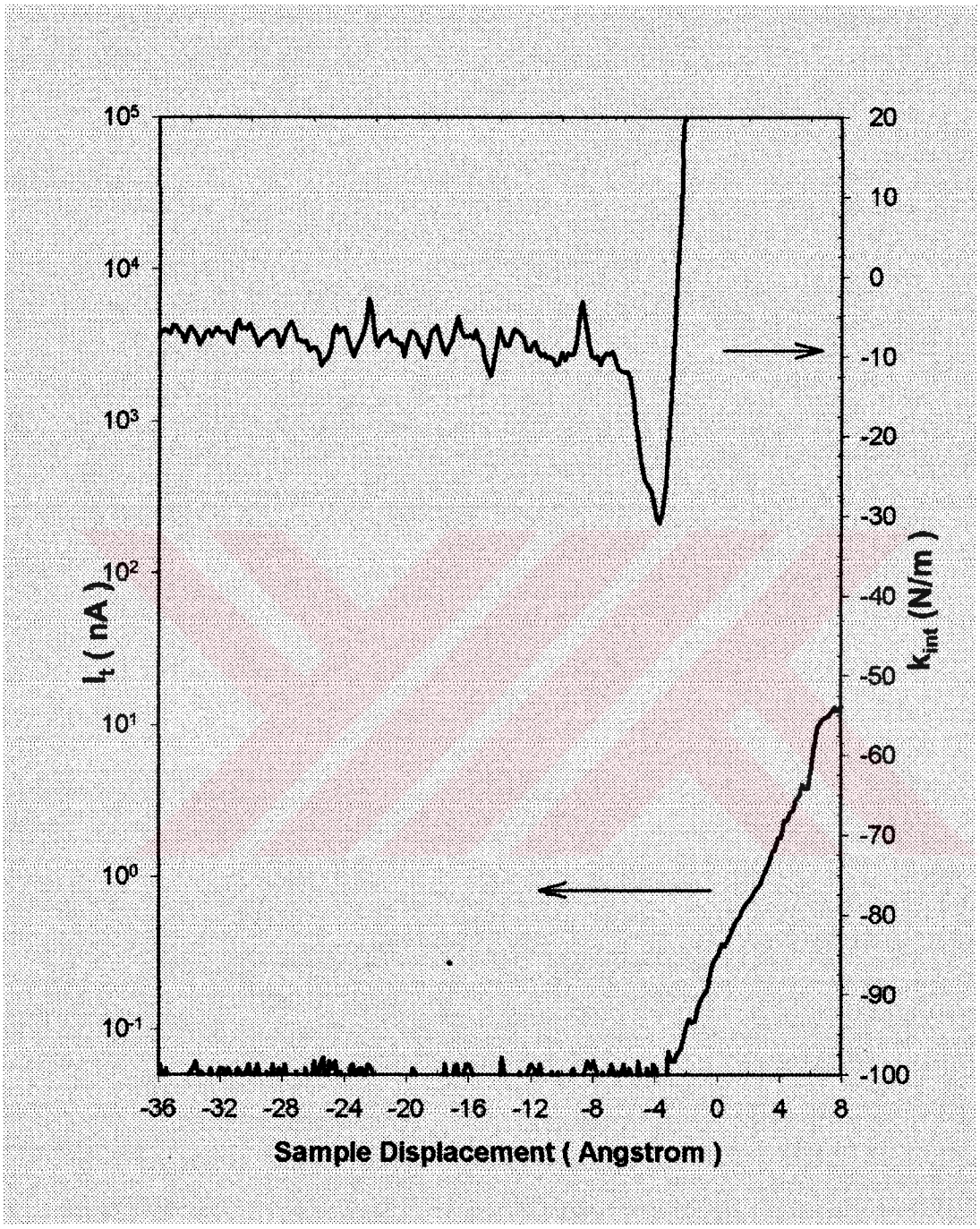

Figure 4.7: *F-d* spectroscopy curve, shows simultaneously tunnel current and force gradient measurement. k_o=160 N/m and A_o= 0.25 Å.

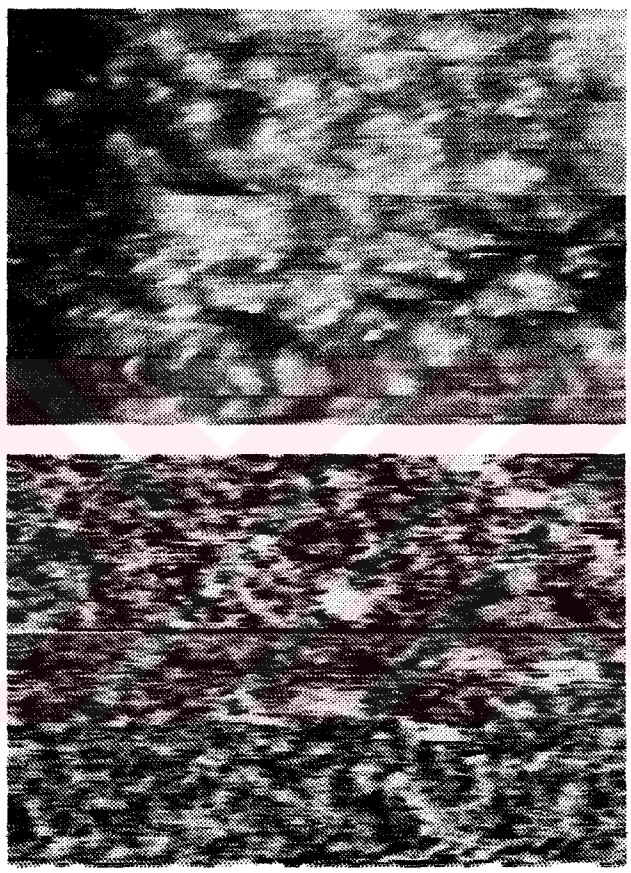

Figure 4.8: Simultaneous STM(top) and force gradient(bottom) images of $\sim$ 0.4 ML Ge on Si(100) 2$\times$ 1 - Image size is 169 $\times$ 249 Å^2. V_{bias}= +1.5 V, I_t= 0.5 nA, A_o= 0.5 Å.

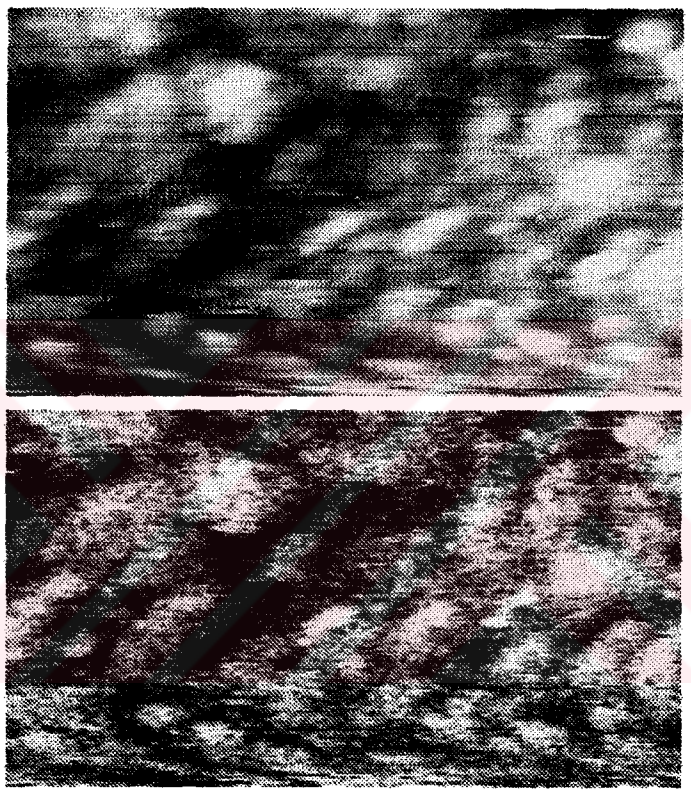

Figure 4.9: Simultaneous STM(top) and force gradient(bottom) images of $\sim$ 0.2 ML Ge on Si(100) 2×1 - Image size is 86×150 Å^2. V_{bias}= +1.5 V, I_t= 0.2 nA, A_o= 0.25 Å.

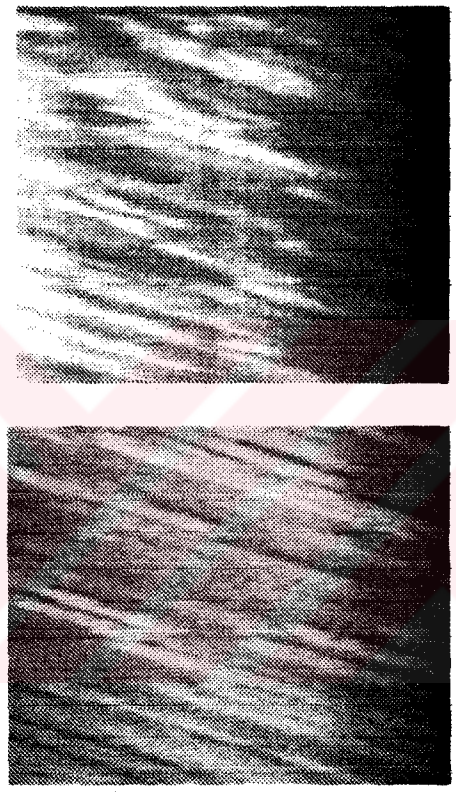

Figure 4.10: Simultaneous STM(top) and force gradient(bottom) images of ~ 0.3 ML Ge on Si(100) 2×1 - Image size is 108×113 Å^2. V_{bias}= +1.5 V, I_t= 0.2 nA, A_o= 0.25 Å.

Chapter 5

Conclusion

In this thesis, the design and construction of an all-fiber interferometer based UHV STM/nc-AFM system as well as initial result on clean Si(001) surface and Ge growth on Si(001) have been described. The new technique, using off-resonance, sub-Ångstrom amplitude is capable to probe short range interaction and therefore true atomic resolution imaging of surfaces quantitatively. It is demonstrated, with this technique measuring the force gradient is straightforward and there is no need to deconvolve frequency shift.

We have investigated, clean Si(001)(2×1) surface with atomic resolution, in STM and force gradient by using UHV STM/nc-AFM simultaneously. The detailed structure of the surface has been analyzed. The images show different contrast which might be due to different tip-surface interaction nature in STM and force gradient imaging.

F-d spectroscopy experiments have also been performed. The change in tunnel current, dc force and force gradient simultaneously measured. The long range and short range interaction F-d curve is obtained with different cantilever.

We have also attempted to use the low amplitude nc-AFM technique to investigate Ge growth on Si(001). A simple Ge evaporator has been constructed to grow Ge on Si(001)surface. Some attempts have started to calibrate the Ge evaporator to deposit desired coverage on the surface. Faint atomic resolution images have been taken simultaneously in STM and force gradient images, but

further experiments are necessary to explain the system in more detail and understand the mechanism of ordering, segregation and tip-surface interaction behavior in the presence of Ge overlayer.

Bibliography

[1] G. Binnig, H. Rohrer, Scanning Tunnelling Microscopy, Helvetica Physica Acta, **55**, 726 (1982).

[2] G. Binnig, H. Rohrer, Ch. Gerber and E. Weibel, Tunnelling Through a Controllable Vacuum Gap, Appl. Phys. Lett., **40**, 178 (1982).

[3] G. Binnig, C. F. Quate, Ch. Gerber, Atomic Force Microscopy, Phys. Rev. Lett., **56**, 930 (1986).

[4] R. W. Carpick, M. Salmeron, Scratching the Surface: Fundamental Investigations to Tribology with Atomic Force Microscopy, Chem. Rev. ,**97**, 1163 (1997).

[5] D. Rugar, P. Hansma, Atomic Force Microscopy, Physics Today, **11**, 23 (1990)

[6] R. Wiesendanger, Scanning Probe Microscopy and Spectroscopy, Cambridge University Press, Cambridge, (1994).

[7] J. Tersoff, D.R. Hamann, Theory of Scanning Tunnelling Microscope, Phys. Rev. B. ,**31**, 805 (1985).

[8] J. Bardeen, Tunneling from many point of view, Phys. Rev. Lett. ,**6**, 57 (1961).

[9] A. Erkan Tekman, Atomic Theory of the Scanning Tunnelling Microscopy, M.Sc.Thesis, Bilkent University, (1987)

[10] T. R. Albrecht, P. Grütter, D. Horne, D. Rugar, Frequency modulation detection using high-Q cantilevers for enhanced force microscope sensitivity , J. Appl. Phys., **69**, 668 (1991).

[11] F. J. Giessibl, Atomic resolution of the Si (111) surface by atomic force microscope, Science ,**267**, 69 (1995).

[12] F. J. Giessibl, Force and frequency shift in atomic-resolution dynamic-force microscopy,Phys. Rev. B. ,**56**, 16010 (1997).

[13] B. Gotsmann, B. Anczykowski, C. Seidel, H. Fuchs Determination of the tip sample interaction force from measured force spectroscopy curves , Appl. Surf. Sci., **140**, 314 (1999).

[14] U. Dürig, Relation between interaction force and ferequency shift in large-amplitde dynamic force microscopy , Appl. Phys. Lett., **75**, 433 (1999).

[15] H. Hölscher, W. Allers, U. D. Schwarz, A. Schwarz, R. Wiesendanger Determination of tip-sample interaction potential by dynamic force spectroscopy , Phys. Rev. Lett. ,**83**, 4780 (1999).

[16] S. H. Ke, T. Uda, K. Terakura, Quantity measured in frequency-shift-mode atomic force microscopy: An analysis with a numerical model , Phys. Rev. B. ,**59**, 13267 (1999).

[17] Y. Sugawara, M. Ohta, H. Ueyama, S. Morita, Defect motion on an InP(110) surface observed with noncontact atomic force microscope , Science ,**270**, 1647 (1995).

[18] S. Kitamura, M. Iwatsuki, Observation of silicon surfaces using ulta high vacuum noncontact atomic force microscope, Jpn. Appl. Phys,**35** pp. L 668 (1996).

[19] M. R. Jarvis, Ruben Peréz, M. C Payne, Can Atomic Force Microscopy Achieve Atomic Resolution in Contact Mode?, Phys. Rev. Lett. , **86**, 1287 (2001).

[20] P. M. Hoffmann, A. Oral, R. A. Grimble, H. Ö. Özer, S. Jeffery and J. B. Pethica Direct measurement of interaction force gradient using an altra amplitude AFM, Proc. R. Soc. A, **457**, 1161 (2001).

[21] A. Oral, R. A. Grimble, H. Ö. Özer and J. B. Pethica, Quantitative atom-resolved force gradient imaging using non-contact Atomic Force Microscopy, *to be appeared in Phys. Rev. Lett.*

[22] R. A. Grimble, Ph. D Thesis, 2000 Oxford University.

[23] H. Ö. Özer, Ph.D Thesis, 2001 Bilkent University.

[24] H. Ö.Özer, M. Atabak, R. Ellialtıoğlu and A. Oral, *to be appeared in Appl. Surf. Sci.*

[25] P. M. Hoffmann, S. Jeffery, A. Oral, R. A. Grimble, H. Ö. Özer and J. B. Pethica Nanomechanics using an Ultra small amplitude AFM, *in preparation.*

[26] S. Jeffery, Ph.D Thesis, 2000 Oxford University .

[27] R. E. Schlier, H. E. Farnsworth, Journal of Chemical Physics, **30**, 917 (1956).

[28] R. M. Tromp, R. J. Hamers and J. E. Demuth, Si(001) Dimer Stracture Observed with Scanning Tunnelling Microscopy,Phys. Rev. Lett. , **55**, 1303 (1985).

[29] D. J. Chadi, Stablilities of Single-Layer and Bilayer Steps on Si(001) Surfaces, Phys. Rev. Lett. , **59**, 1691 (1987).

[30] D. Pan, Appl. Phys. Lett. ,**73**, 1973 (1998).

[31] B. S. Swartzentruber, Y. W. Mo, M. B. Webb and Max Lagally, Scanning Tunnelling Microscopy Studies of Stractural Disorder and Steps on Si Surface, Journal of Vacuum Science and Tech. , **A(7)**, 2901 (1989).

[32] J. Knall and J. B. Pethica, Growth of Ge on Si(001) and Si(113) studies by STM, Surface Science , **265**, 156 (1992).

[33] Y. M. Mo and M. G. Lagally, Anisotropy in surface migration of Si and Ge on Si(001), Surface Science , **248**, 313 (1991).

[34] A. Oral and R. Ellialtıoğlu, Initial stages of SiGe Epitaxy on Si(001) studies by Scanning Tunnelling Microscopy, Surface Science , **323**, 295 (1995).

[35] Max Lagally, Atomic motion on surface, Physics Today, **11**, 24 (1999).

[36] A. Oral, Ph.D Thesis, 1994 Bilkent University.

[37] G. Neubauer, S. R. Cohen, G. M. McClelland, D. Horne and C. Mate, force microscopy with a bidirectional capacitance sensor, Rev. Sci. Instrum. ,**61**, 2296 (1990).

[38] G. Meyer, N. M. Amer, Novel Optical approach to atomic force microscopy, Appl. Phys. Lett., **53**, 1045 (1988).

[39] W. Mönch, Semiconductor Surface and Interfaces, Springer- Verlag , (1993).

[40] A. Ishizaka, Y. Shiraki, Low Tempreature surface cleaning of Silicon and Its Aplication to Silicon MBE, Journal of Electrochemical Society, **133**, 666 (1986).

[41] EPOTEK H21D Conductive Adhasive, Caburn-MDC Ltd., The Old Dairy Street, Glynde, East Sussex, BN8 6SJ UK.

[42] ILFORD PQ Universal Photographic film developer.

[43] D. Rugar, H. J. Mamin, R. Erlandsson, J. E. Stern and B. D. Terris,Force microscope using a fiber-optic displacement sensor, Rev. Sci. Instrum., **59**, 2337, (1988)